minerals

MDPI

Article

Structural Analysis and Paleostress Evolution in the Imiter Silver Mining Region, Eastern Anti Atlas, Morocco: Implications for Mineral Exploration

Youssef Atif [1,2], Abderrahmane Soulaimani [1], Abdelhak Ait Lahna [1], Driss Yaagoub [3], Nasrrddine Youbi [1,4], Amin Beiranvand Pour [5,6,*] and Mazlan Hashim [6]

1 DLGR Laboratory, Department of Geology, Faculty of Sciences-Semlalia, Cadi Ayyad University, Prince Moulay Abdellah Boulevard, P.O. Box 2390, Marrakesh 40000, Morocco
2 Managem, Twin Center, Tour A, Angle Bd Zerktouni-Abdelkarim Khattabi, BP 5199, Casablanca 20100, Morocco
3 Intelligent Systems, Georesources & Renewable Energies Laboratory, Faculty of Sciences and Techniques, Sidi Mohammed Ben Abdellah University, BP 2202, Route d'Imouzzer, Fez 30050, Morocco
4 Faculty of Geology and Geography, Tomsk State University, 36 Lenin Ave., 634050 Tomsk, Russia
5 Institute of Oceanography and Environment (INOS), University Malaysia Terengganu (UMT), Kuala Nerus, Kuala Terengganu 21030, Malaysia
6 Geoscience and Digital Earth Centre (INSTeG), Research Institute for Sustainable Environment, Universiti Teknologi Malaysia, Johor Bahru 81310, Malaysia
* Correspondence: beiranvand.pour@umt.edu.my or beiranvand.amin80@gmail.com; Tel.: +60-9-668-3824; Fax: +60-9-669-2166

Abstract: Development and concentration of many ore deposits at the regional and district scales closely depend on structural geology, especially in polydeformed basements. The superposition of many deformation periods highlights the complexity of the structural context and expected potential location of mineralization zones. The formation and concentration of hydrothermal ore deposits is highly dependent on structural controls. On the NE flank of the Saghro massif (Eastern Anti-Atlas, Morocco), the Imiter silver mining region has been affected by multiple tectonic events since the Precambrian and throughout the Phanerozoic. In this investigation, a structural analysis of the different geological units revealed multi-stage deformation, beginning with the late Pan-African-Cadomian event, and ending with the last Cenozoic exhumation of the area. At least eight tectonic regimes have been identified. The Imiter basement, formed by the Cryogenian-early Ediacaran "flysch-like" Saghro Group, has been folded in low-grade metamorphic conditions, followed by an ENE-WSW brittle compressive event. These deformations occurred before to the early Ediacaran during the compressional and/or transpressional late Pan-African-Cadomian events (600–580 Ma). The unconformably overlaying deposition of the late Ediacaran Ouarzazate Group takes place in a WNW-ESE extensional setting and then involved in a NNW-SSE compressional event that occurred concurrently with a regional exhumation and erosion stages. A similar extensional event appears to have controlled the middle Cambrian sedimentation, the oldest Paleozoic deposits in this area. During the late Carboniferous, Variscan shortening was recorded by NW-SE transpressional deformation responsible for combined dextral strike-slip and southward thrusts. The Imiter silver mining region is part of the Moroccan Sub-Meseta Zone along with Paleozoic inliers of the Skoura and Tamlelt on the southern side of the High Atlas. The Mesozoic evolution began with the Late Triassic NNW-SSW transtensional tectonic regime with a northeast trending CAMP (Central Atlantic Magmatic Province) dyke during the Pangea breakup. Ultimately, the Imiter silver mining region experienced NNW-SSE Atlasic shortening during the uplift of the adjacent High Atlas. Over time, the direction of implemented tectonic stress and its effect on various geological units can elucidate the relationship between tectonism and hydrothermal silver mineralization in the Imiter region. In conclusion, structural analysis and investigation of paleostress development can be one of the most important factors for successful exploration plan and resource recovery in the Imiter region. An analysis of geological structures in determining feasible mineralization zones is crucial for future safe mining operation in the study area and can be extrapolated to other ore mining regions.

Citation: Atif, Y.; Soulaimani, A.; Ait Lahna, A.; Yaagoub, D.; Youbi, N.; Pour, A.B.; Hashim, M. Structural Analysis and Paleostress Evolution in the Imiter Silver Mining Region, Eastern Anti Atlas, Morocco: Implications for Mineral Exploration. *Minerals* **2022**, *12*, 1563. https://doi.org/10.3390/min12121563

Academic Editors: Huan Li and Han Zheng

Received: 10 November 2022
Accepted: 2 December 2022
Published: 4 December 2022

Keywords: structural analysis; paleostress configurations; Imiter inlier; silver mineralization; saghro inlier; Morocco

1. Introduction

Geological structures serve as reminders of significant Earth history events. They can be of economic significance because they frequently serve to concentrate ore deposits. Porphyry copper, Volcanic Massive Sulfide (VMS), Iron oxide-copper-gold (IOCG), skarn, hydrothermal and epithermal deposits are controlled by specific structural/lithological settings (e.g., [1–7]). Accordingly, the geological and geophysical (e.g., [8]) of a variety of ore deposits depends strongly on the analysis of geological structures at the regional and district scales.

Determining the time of significant structural events is very helpful for analyzing and classifying fluid conduits and building a genetic model for ore deposition, e.g., [9–12]. Knowledge of the structural trends of the mineralization processes is necessary for the accurate identification, quantification, and utilization of ore deposits. This is particularly crucial for ores placed in polydeformed basements, where the superposition of many deformation periods highlights the complexity of the structural context. The formation of hydrothermal ore deposits is typically related to geological structures [7,9,12–15]. The prevalence of structural controls, in which a frequently multi-scale network of previously existing structural discontinuities in the host rocks forms a pre-established plumbing system for circulation and entrapment of hydrothermal fluids, and this depends on the tectonic regime in which the mineralizing phenomena occur [11].

In the northwestern part of the West African Craton, the Anti-Atlas Mountains in sub-Saharan Morocco has been structured during four main orogenic cycles, Eburnean, Pan-African, Variscan and Alpine orogenesis. To its east, the Saghro massif displays a Neoproterozoic basement unconformably overlapped by the late Ediacaran volcaniclastic Ouarzazate Group, then by a thick Paleozoic sedimentary cover. The Imiter region is known by the Imiter world-famous silver mine, located on the northeast side of the Saghro massif [16–24]. Its basement outcropping at the Imiter inlier are folded "flysch-like" Saghro Group sediments. The Saghro Group is currently considered to be Cryogenian-late Ediacaran in age, folded by synmetamorphic deformation before to the unconformably overlaying deposits of the early Ediacaran Ouarzazate Group [23,25,26]. The latter is dominated by volcanic, volcano-clastic, and equivalent plutonic and subvolcanic rocks [24,27]. The still debated geodynamic context of the early Neoproterozoic Saghro and Ouarzazate Groups belongs the late Pan-African-Cadomian orogeny [24,28,29].

Cambrian marine sedimentation began in the Imiter region with the middle Cambrian siliciclastic sediments and continued into the Carboniferous [16]. Paleozoic sedimentary rocks preserved at the north of Imiter area are affected by dextral E-W south-verging thrust faults within the crystalline basement [30,31]. This "thin-skinned tectonic" deformation during the Variscan orogeny is similar to the other northern Sub-Mesetian belts, including the Skoura and Tamlelt domains on the south side of the High Atlas [32]. Since then, the Imiter region has undergone Atlas-Alpine evolution, characterized first by late Permian to Late Triassic crustal extension and then by vertical motion before the last exhumation during the Neogene compressions that lead to the High Atlas uplifts.

From the above-mentioned long-term development, the Imiter silver mining area has experienced several compression and extensional tectonic events from the late Pan-African period. This paper aims to decipher these continuous tectonic structures associated with the subsequent synmetamorphic/brittle deformation events. Structural measurements allow specifying the direction of tectonic stress and its effects on different geological units over time. In addition, the results of this structural inventory are critical to further understanding the relationship between subsequent tectonic activity and silver ore deposits in the Imiter districts and further out in the eastern Anti-Atlas belt.

2. Geological Setting

2.1. The Anti-Atlas Belt

The Anti-Atlas basement consists of Paleoproterozoic rocks (≈2.20–2.07 Ga) in the western and central inliers (Bas-Draa, Ifni, Kerdous, Tagragra d'Akka, Tagragra de Tata, Agadir Melloul, Iguerda and Zenaga), south of the Anti-Atlas Major Fault [23,27,33–38], (Figure 1). The Paleoproterozoic consists of metasedimentary rocks, paragneiss, migmatite and granite with U-Pb zircon ages of 2200 to 2030 Ma (e.g., [38]). The Paleoproterozoic basement, also includes the mafic dikes of about 2040 Ma at Tagragra of Tata [35] and Zenaga inlier [39].

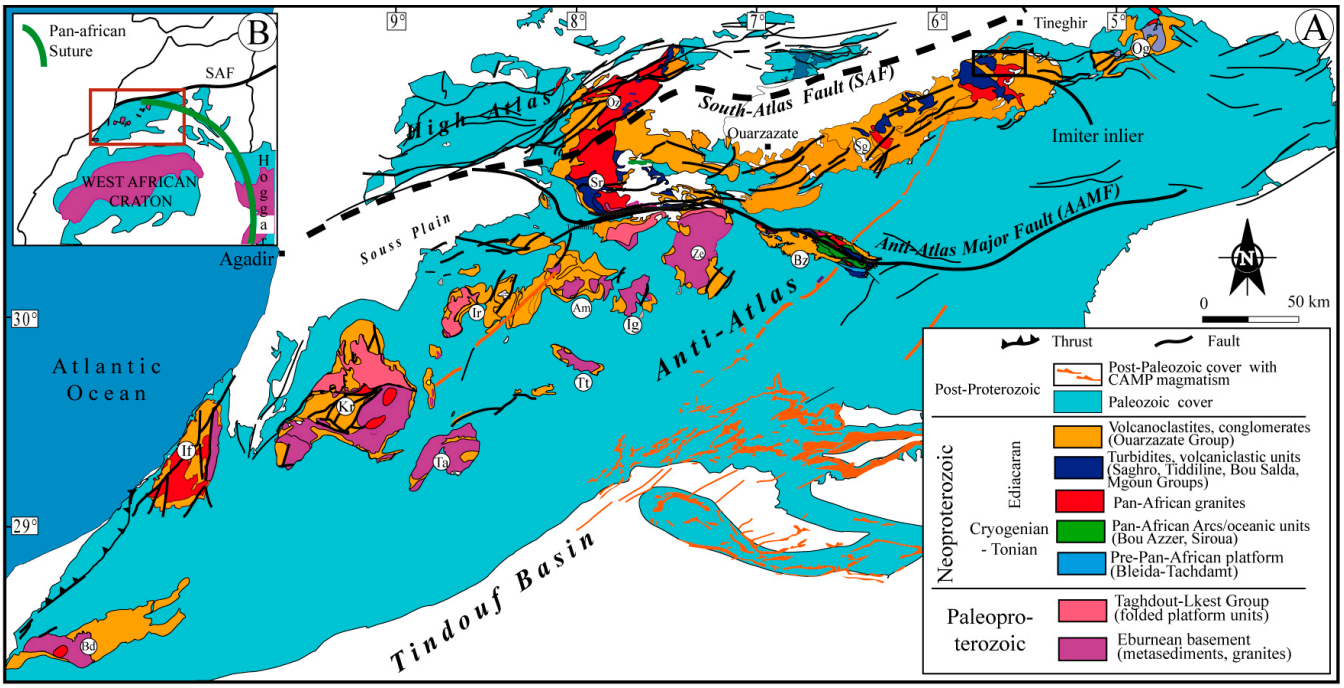

Figure 1. (**A**) Simplified geological sketch map of the Anti-Atlas belt (after [29]). (**B**) The inset shows the location of the Anti-Atlas domain north of the West African Craton. Abbreviations: Og = Ougnat; Sg = Saghro; Bz = Bou Azzer; Ze = Zenaga; Tt = Tagrara Tata; Sr = Sirwa; Oz = Ouzallarh; Ig = Ighouda; Am = Agadir Malloul; Ir = Ighrem; Ta = Tagrara Akka; Kr = Kerdous; If = Ifni; Bd = Bas Draa.

The Eburnean basement lies unconformably beneath the Taghdout-Lkest carbonates and quartzites series exposed to the central and western Anti-Atlas. These units, previously thought to be Neoproterozoic pre-Pan-African deposits, are now thought to be late Paleoproterozoic platform, nearly 1Ga earlier than previously thought, because of the doleritic dykes and sills of 1710–1639 Ma crosscut the Taghdout-Jbel Lkest Group [40,41].

Mesoproterozoic rocks or events are almost non-existent in the Anti-Atlas, which experienced prolonged quiescence between 1.7 and 1.0 Ga (e.g., [23]). At Zenaga and Bas-Draa inliers, only intraplate mafic dykes have been detected based on U-Pb dating of baddeleyite and zircon (1416–1380 Ma) [39,41–43]. The Anti-Atlas Neoproterozoic sequences are subdivided into four groups [20,23], namely: (i) Tachdamat-Bleida Formation, 883 Ma [40], composed of quartzites, carbonates, and basalts deposited earlier on the northern rifted margin of the (Western African Craton) during the onset of Pan-African event [20,44,45]; (ii) the Bou-Azzer-Siroua Group, consisting of a complex mixture of ophiolitic slices and arc remnants [28,37,46–50]; (iii) the late Ediacaran turbiditic and clastic series of the Saghro Group [25,26]. The Saghro Group is located at the base of Bou Salda, M'Goun, and Tiddiline Groups; and (iv) the widely distributed early widespread Ediacaran Ouarzazate Group, consisting of volcanic, volcano-clastic, and equivalent plutonic and subvolcanic rocks [24,27].

The Ouarzazate Group of the late Ediacaran was para-conformably covered by Tata and Taroudant Groups deposits [24,51], marking the beginning of the long transgressive Paleozoic cycle [52–54]. At the end of the Carboniferous, Anti-Atlas suffered from moderately thick-skinned tectonics caused by the Pangean assembly during the Variscan orogeny [32,55,56]. During Late Triassic, the Anti-Atlas was influenced by Atlas-Alpine tectonics, first characterized by the NNW-SSE extension event relative to the central Atlantic opening [54,57]. At this time, the Anti-Atlas is considered the uplifted southern shoulder of the Atlas rift, bisected by NE-trending dikes and sills of the CAMP. Thereafter, the entire Anti-Atlas area underwent vertical movements in the Mesozoic and Cenozoic, and was finally exhumed in the Neogene; coinciding with the rise of the High Atlas [58–60].

2.2. The Saghro Massif and Imiter Inlier

The Jbel Saghro massif belongs to the eastern Pan-African domain of the Anti-Atlas, northeast of the AAMF (Anti-Atlas Major Fault) [33], (Figure 1). To its northeast is the Imiter area for the huge Imiter silver deposit, southwest of the city of Tinghir (Figure 2). The Eburnean basement is missing from the Saghro massif outcrops. Nonetheless, Paleoproterozoic inherited zircons from various pan-African magmatism demonstrate its potential existence underneath [22,61]. The old rocks of the Saghro massif (Saghro Group) consists of a thick metasediment deformed and metamorphosed under low greenschist (albite-epidote) conditions (e.g., [24,62–65]) The Saghro Group rocks are exposed from west to east in several sub-inliers of Sidi Flah–Bouskour, Kelaa Mgouna, Boumalne, and Imiter [20,22–24,66,67].

The Saghro Group is composed of weakly metamorphosed sandstones and black shales containing inter-bedded synsedimentary subaqueous mafic lavas at various level within the Kelaat Mgouna, Sidi Flah, and Boumalne inliers [67]. These volcanic rocks represent continental tholeiites and alkaline basalts, typical of intracontinental rifts in a back- arc setting [66,68,69]. In the triangular-shaped Imiter inlier [16,70], the basement of the Saghro Group (Imiter sequence) consists of four units involved in a NE-SW anticline. They are in the ascending order (Figure 3): (i) the black shale unit; (ii) the dominant metasandstone unit; (iii) the metasandstone-metapelite unit with dominant metasandstone; and (iv) the metasandstone -metapelite unit with dominant metapelites [71].

The Tectonic setting of the Saghro Group in the Pan-African framework remains poorly constrained [25,26]. The Saghro Group deposits are interpreted to have formed in an extensive back-arc environment [66,72]. Its lower part is not exposed, it may be Cryogenian of age, and its maximum deposition age is estimated to be about 620–610 Ma according to recent detrital zircon dating [26,73–75]. Note that, like all Saghro and Ougnat massifs to the east of Anti-Atlas, the Imiter Saghro Group is affected by a regional syn-metamorphic deformation, that occurred in a low-grade metamorphic conditions, previously ascribed to the main Cryogenian Pan-African deformation (650 Ma), known along the central Anti-Atlas suture [17,68,76]. The younger maximum depositional age of the Saghro Group is more consistent with younger deformation during the late Pan-African-Cadomian event around 600 Ma [25,26].

Over most of the largest part of the Saghro massif, the Saghro Group metasediments are unconformably covered by volcanic and volcaniclastic rocks of the late Ediacaran Ouarzazate Group (575–546 Ma) begins by a polygenic conglomerate. The Ouarzazate Group has a wide variety of mafic, intermediate, and felsic dikes (dolerite, andesite, andesitic basalt, and rhyolite), and plutonic rocks with highly potassic calc-alkaline affinity, dating from 582 to 543 Ma (i.e., Taouazzak granodiorite) [17–24,40,71,77–79]. Around the Saghro massif, the Ouarzazate Group is overlain with a more or less obvious angular unconformity by Tata and Taroudant Groups deposits [24,51], marking the beginning of the Paleozoic transgressive cycle [52–54].

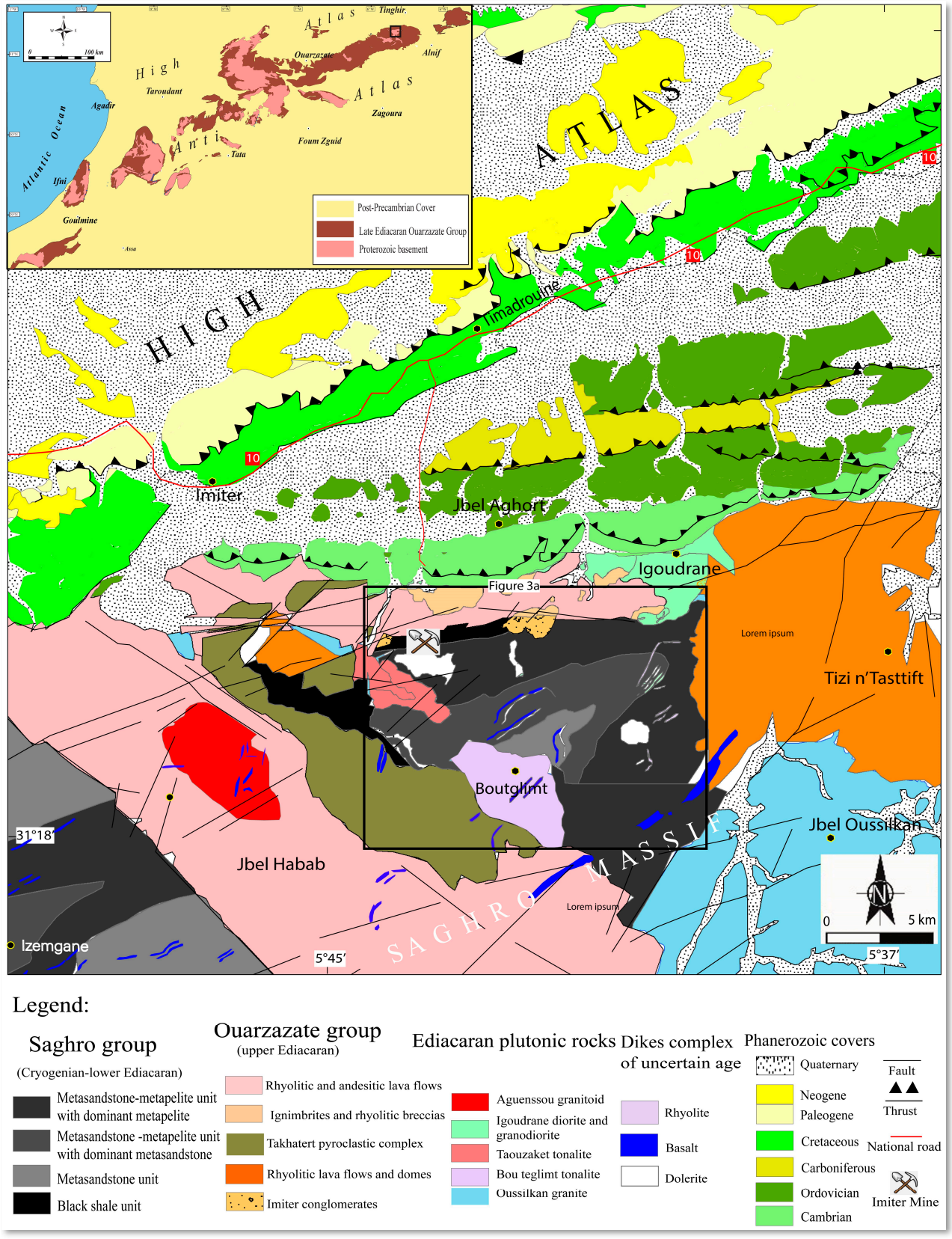

Figure 2. Simplified geological sketch map of the Imiter and Boumalne inliers and surrounding geological units (modified after [71,80]), the inset shows the location of Imiter area northeast of the Anti-Atlas.

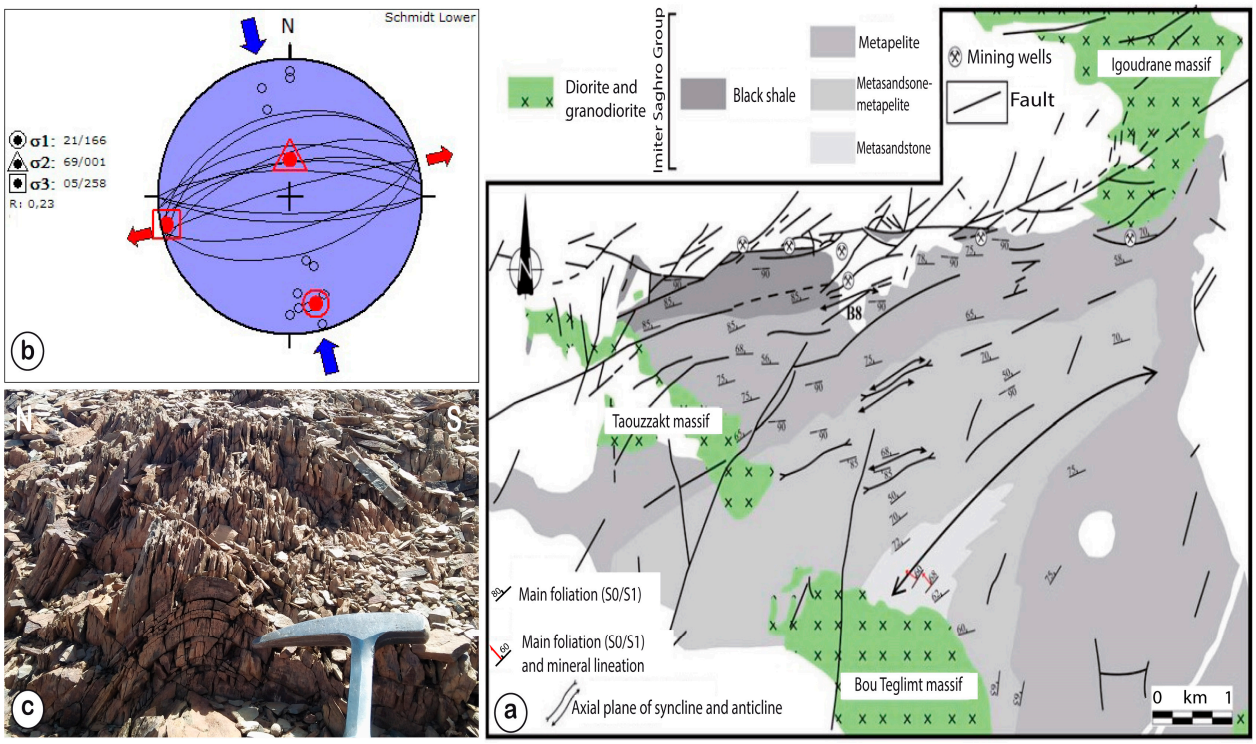

Figure 3. (**a**) Structural map of Imiter's basement, showing foliation and fold orientation at the map scale [81]; (**b**) stereographic projection of foliation planes, poles, and poles density; (**c**) photograph of an upright foliation fold which affecting the metasediments of the Saghro Group.

The Paleozoic series in the Imiter inlier begins directly with the middle Cambrian formations. The base term is a metric bar of lumachellic conglomerate with limestone intercalations whose exact age has not yet been determined. An old estimate gives a Georgian age [70]. It is surmounted by thick sandstone-pelitic formations of the Tissanian (middle Cambrian).

During the Variscan orogeny, Paleozoic sedimentary rocks from the middle Cambrian to Carboniferous were pushed southward onto the Precambrian basement [30,31]. Variscan south-verging thin-skinned tectonic deformation was characteristic of the Sub-Mesetian Zone, including Skoura and Tamlelt regions [32]. The eastern Anti-Atlas post-Variscan history from apatite fission-track and zircon U-Th/He studies shows evidence of a multi-phase Meso-Cenozoic vertical motion history [58]. After serving as the southern shoulder of the Triassic Atlas rift, the region experienced a Neogene dextral transpressional pattern associated with the sub-meridian shortening leading to the High Atlas uplift.

3. Methodology

Geometric analysis of faults is based on field observations and structural measurements of various formation in the Imiter area, including Cryogenian, Ediacaran, late Paleozoic, and Cenozoic formations. In the metamorphic basement, ductile structures, as foliations and fold axes, are systematically measured and reported in the structural map of the Imiter inlier, allowing the geometry and orientation of the finite strain trajectories to be discussed. On the other hand, the separation and chronology of the subsequent brittle deformations are based on tectoglyphes analysis of different fault, cross observations, superposition of striae on the same fault incompatibility of parallel fault displacement, synsedimentary or synvolcanic faults. The measures are handled by the program Win Tensor [82–85]. The procedure is based on the rationale of [86,87].

Numerical methods of tectonic stress inversion correspond to methods of understanding the faults data received through fault slides that are relevant to the geological setting. It is based on the assumption of Bott, 1959 [88–90], that the stress field is stable and uni-

form in space and time. In the stress tensor, the inversion method is associated with the following main parameters: the orientation and the strength of the principal stress axes σ1, σ2, σ3 with $\sigma1 \geq \sigma2 \geq \sigma3 \geq 0$, and the aspect ratio of the principal stress axis ellipsoid $R = (\sigma2 - \sigma3)/(\sigma1 - \sigma3)$ where $0 \leq R \leq 1$ [89,91–94]. All results were represented in the stereograms using the lower hemisphere.

4. Structural Analysis of the Imiter Area

As mentioned above, the Imiter geological units can be divided into two rheological units: (i) the low metamorphic basement, represented by the "flysch-like" Cryogenian-Ediacaran Saghro Group; and (ii) the early Ediacaran volcano-sedimentary Ouarzazate Group and late Paleozoic series. Structural analysis of the region revealed at least eight episodes of multistage deformation, beginning with the late Pan-African-Cadomian event, and ending with the last Cenozoic exhumation of the region, including the late Carboniferous Variscan deformation. Note that the Imiter basement exhibits ductile synmetamorphic deformation, while brittle deformations affect both the basement and the overlying cover.

4.1. Ductile Deformation of the Saghro Group Basement (Dp1)

The outcrop of the Imiter Saghro Group basement in the Imiter subinlier occurs in a triangular flat area (Imiter inlier) as a cartographically folded metasedimentary series formed by an alternating sequence of metasandstone, quartzite, and shale. These metasediments preserve the Bouma-type turbidites, thought to be seafloor debris cones at the bottom of a continental margin [72,95]. The siliciclastic strata in the Imiter Saghro Group show normal north-south polarity, with thick metasandstone beds in the south and a gradual decrease in thickness toward the north. The Imiter Saghro Group terminates in the north in the anoxic black shale formation where most of the giant Ag-Hg Imiter deposit is located.

The Folded Saghro Group in the Imiter Zone was affected by synmetamorphic folding occurred during low-grade greenschist metamorphism [17,76], corresponding to the last compressional and/or transpressional event of the Pan-African orogenic cycle in the Anti-Atlas [25,26]. Generates at the outcrop scale, foliation planes well developed in the fine-grained lithology and less developed in the competent metasandstones with the neoformation of phyllosilicate minerals. The foliation is oriented from N30 to N80, mainly down to NNW (Figure 3a,b), the heterogeneous foliation corresponds locally to the axial plane of folds on a metric scale with direction from N030° to N060° E (Figure 3c). At the microscale, the coarse lithology shows lithoclasts of quartz, quartz + plagioclase and quartz + Kfeldspar rubble from granitic and/or volcanic sources. Slaty cleavage is observed in the fine-grained lithology.

4.2. Brittle Deformation

Following the synmetamorphic deformation recorded in the basement, a series of brittle tectonic episodes affected the Imiter region, leading to the continued development and/or reactivation of brittle structures in the basement and overlaying cover. The structural analyses of these fault networks were performed in different lithofacies of the Precambrian, Paleozoic, and Cenozoic series. To provide a holistic view, the structural map in Figure 4 below, generated from analysis of field data and satellite images, shows the major fault system in the Imiter area from either side of the Imiter fault.

4.2.1. Brittle Deformation in the Neoproterozoic Basement (Dp2)

The structural analysis of Imiter inlier's Saghro Group fault network allows detection NW-SE reverse faults and sub-meridian reverse faults with strike-slip components (Figure 5a). Construction states are compatible with the sub-vertical σ3 stress axis (N121, 81ESE), the horizontal σ2 stress axis (N157-07NNW) and the horizontal maximal σ1 stress axis (N66-05WSW). R ratio R = 0.75; this shows that $\sigma1 \approx \sigma2$. Thus, the major ENE-WSW compression axis was associated with a minor NNW-SSE compression axis (Figure 5b). These faults highlight a specifically identified ENE-WSW compression event in the base-

ment and absent in the overlying volcanosedimentary Ouarzazate Group and Paleozoic cover. Thus, these faults are associated with brittle events during exhumation and erosion periods between the early and late Ediacaran.

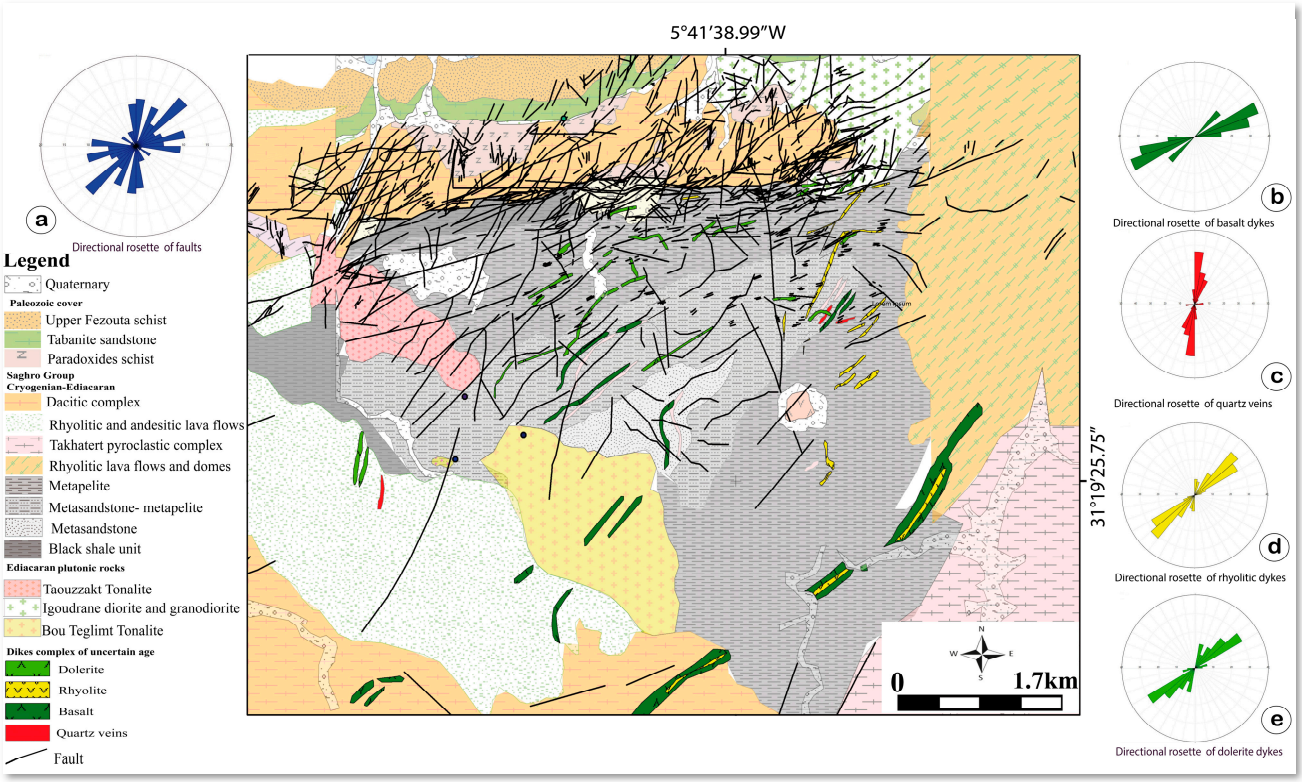

Figure 4. Structural map showing the major fault systems in the Imiter area; (**a**–**e**) respectively show directional rosettes of faults, basaltic dykes, quartz veins, rhyolitic dykes, and dolerite dykes.

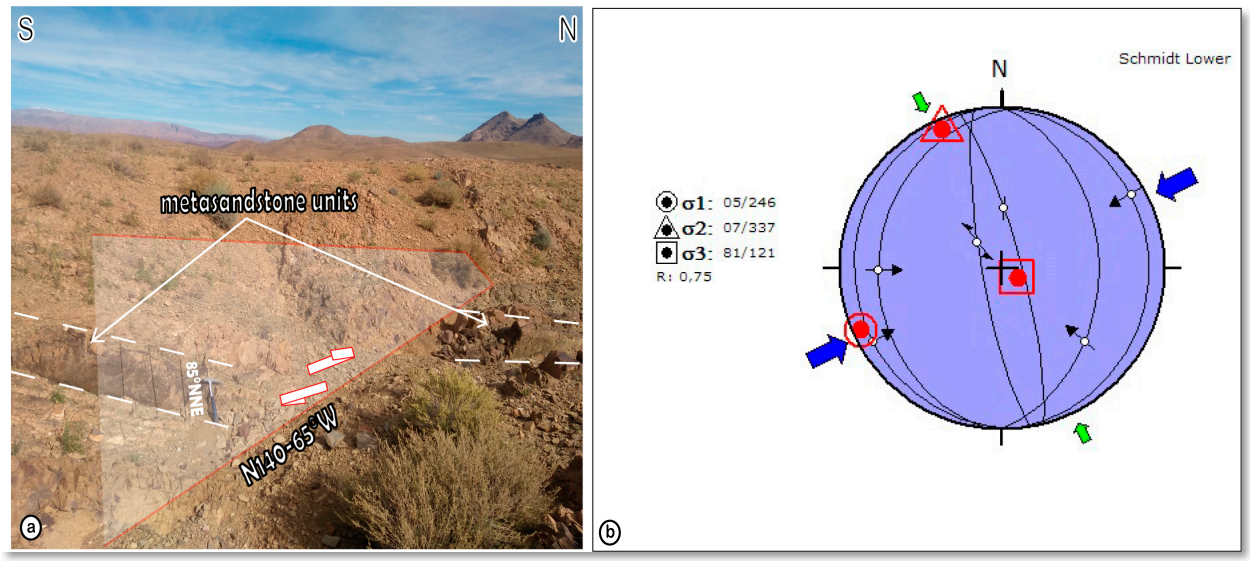

Figure 5. (**a**) Field photo showing a NW-SE strike-slip affecting the black shales units of the Saghro Group. (**b**) Stereographic projection of the fault analysis and the interpreted stress axis during the brittle deformation of the Saghro Group basement.

4.2.2. Tectonic Events Recorded in the Late Ediacaran

Structural analysis of the faults affecting the upper Ediacaran succession allowed us to identify at least two Ediacaran tectonic events that did not affect the overlying Paleozoic cover.

- Syn-sedimentary WNW-ESE extensive stage (***Dp3***)

The lithostratigraphic units of the Ouarzazate Group, more specifically the Imiter conglomerate, are controlled by syndepositional N15° to N30° normal faults (after horizontal tilting of S0). These faults are compatible with a horizontal NW-SE trend σ3 axis (N123°-01° WNW), σ2 stress direction N33° dip of 12° SSW and sub-vertical σ1 axis (N36°-78° SSW) (Figure 6a). The R ratio = 0.42 means σ2 ≈ (σ1 + σ3)/2 (Figure 6b).

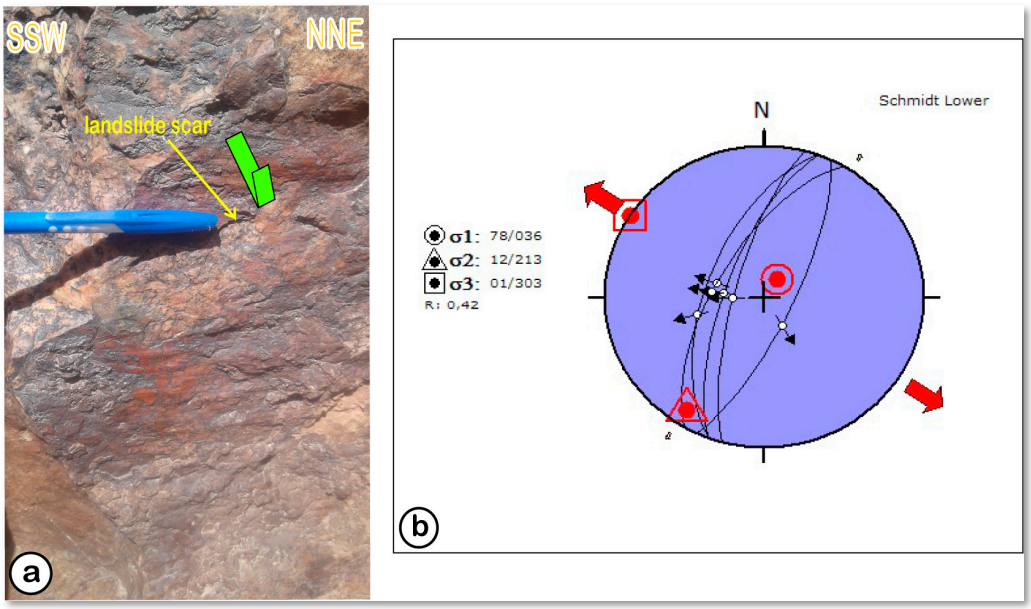

Figure 6. (**a**) Field photograph showing a NNE-SSW normal faults; (**b**) stereographic projection of the fault analysis and the interpreted stress axis during the during synsedimentary and syn-volcanism early Ediacaran extension.

- The NNW-SSE compressive stage (***Dp4***)

This stage corresponds to E-W dextral strike-slip faults with small reverse components crosscutting the Cryogenian basement and Ediacaran volcanic rocks (Figure 7b). These faults are covered by the lower units of the middle Cambrian and are therefore active before the deposition of the middle Cambrian units. The tectonic event was caused by a stress field with a sub-horizontal σ1 axis at N148°-05° NW, a σ2 axis at N066°-58° ENE and a minimal stress axis σ3 at N055°-31° WSW. The R ratio = 0.5; this shows that σ2 ≈ (σ1 + σ3)/2. This compression phase results in a reverse fault associated with strike-slip faults with reverse component (Figure 7a).

4.2.3. Tectonic Events Recorded in Cambrian and Post-Cambrian Series

The Paleozoic units the Imiter area begin with the middle Cambrian series. At the base of this series below a meter-wide lumachellic conglomerate with interbedded limestone layers deposited, in unconformity on the Ouarzazate Group. It is covered by thick middle Cambrian siliciclastic formation which dips from 15° to 30° to the North. Several striated faults have been measured in Cambrian formations (Brèche à Micmacca, marls with Paradoxides and Tabanit sandstones). These faults show various orientations and have been reactivated over time. They are locally filled with hydrothermal silica and carbonate recrystallization, and the host rock is strongly altered or even brecciated.

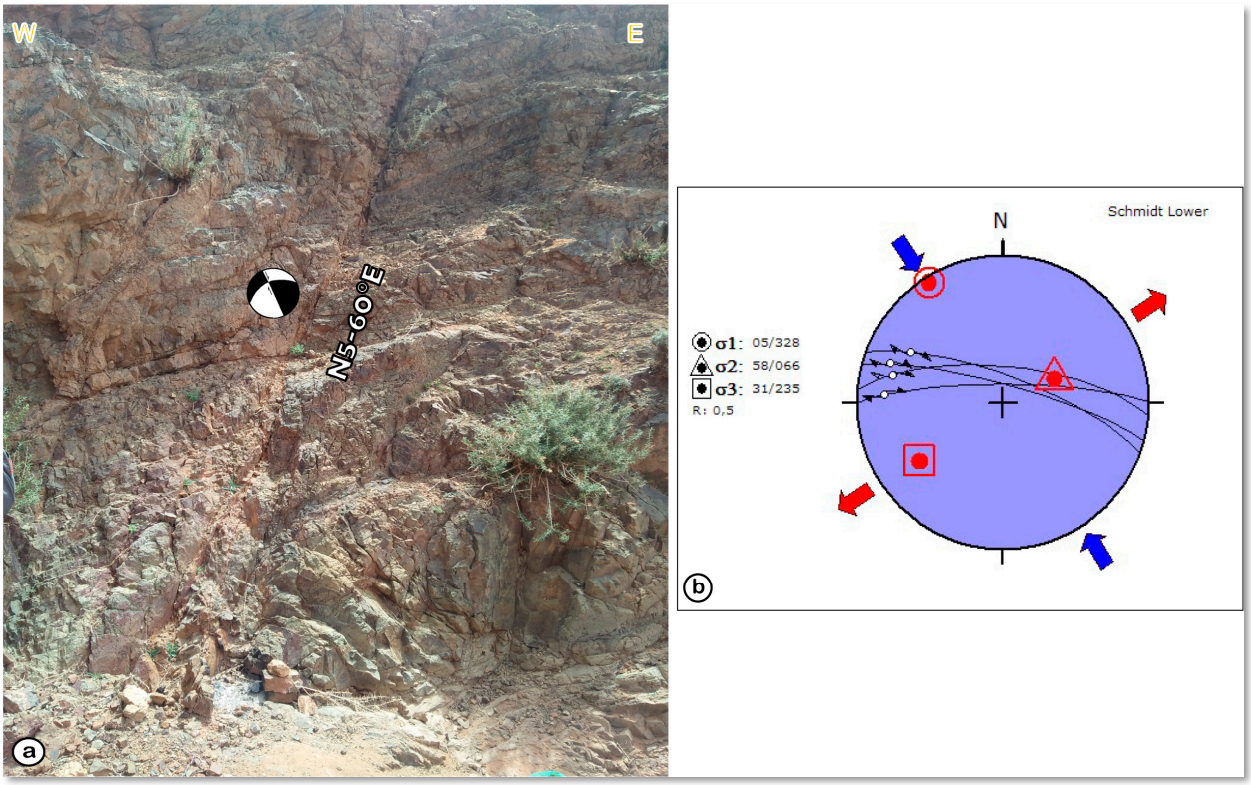

Figure 7. (**a**) Field photograph showing a dextral strike-slip affecting the Ouarzazate Group volcanicanosedimentary units. (**b**) Stereographic projection of the fault analysis and the interpreted stress axis during the compressive brittle deformation of the early Ediacaran.

- The NNW-SSE Cambrian extensional stage (***Dc***)

Synsedimentary N060° to N075° normal faults remain in the Cambrian sediments (Figure 8a–c). These values take into account the S0 correction (tilting S0 to the horizonal and rotating all fault plane measurements by the same angle). From these measurements, we deduce that the σ3 stress axis was horizontal with direction N164°-10° NNW, the σ2 direction is N076°-080° ESE, and the maximum stress axis σ1 was oriented N024°-77° WSW (Figure 8d). The R ratio = 0.56; this shows that $\sigma 2 \approx (\sigma 1 + \sigma 3)/2$.

- The NW-SE compressive stage (***Dv***)

At this stage, the NE-SW faults were reactivated into reverse faults, the E-W faults were reactivated as dextral strike-slip faults (Figure 9a) and the N-S faults were reactivated as sinistral strike-slip faults (Figure 9b). These fault motions are compatible with paleostress field such as the σ1 axis is horizontal at N146°, the σ2 axis is at N057°-32° SW and the σ3 axis at N054°-58° NE (Figure 9c). The R ratio = 0.28. This tectonic stage may correspond to the major Variscan event described in the Anti-Atlas and elsewhere in Morocco (See Section 5 discussion below).

- The N-S to NW-SE extensional tectonic and the collapse of the Imiter fault (***Dt***)

During this deformative phase, the NE-SW faults were reactivated as normal faults and N-S faults were reactivated as dextral strike-slip faults with a normal component (Figure 10). This configuration is compatible with a stress field where the σ1 axis is sub-vertical and oriented N047°-68° NE, the σ2 axis is N051°-22° SW and the σ3 axis is N140°-01° SE (Figure 10d,e). The R ratio = 0.38. So $\sigma 2 \approx (\sigma 1 + \sigma 3)/2$.

Meanwhile, the ENE-WSW to E-W oriented faults (including great Imiter and related faults) showed normal offset. This is compatible with a stress field with the σ3 axis oriented at N003°-08° N, the σ2 axis at N078°-48° W and the σ1 axis at N094°-40° E (Figure 10e). R ratio = 0.85, which means that the value of σ2 is close to σ1. Since the σ1 and σ2 axes dip at

40° and 48°, respectively, the normal offset of the Imiter fault is associated with apparent collapse. The value of the R ratio also means that normal faults can be associated with extensional strike-slip faults (associated with a transtensional tectonic setting).

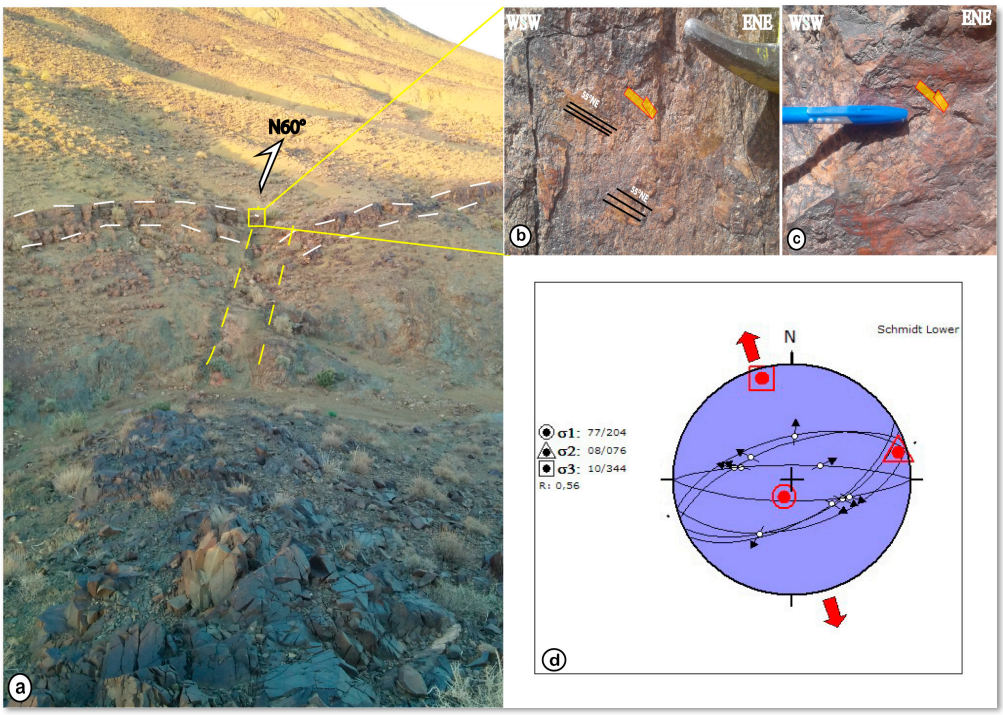

Figure 8. (**a**–**c**) Field photographs show a normal fault crosscutting the Micmacca breccia at the base of the middle Cambrian. (**d**) Stereographic projection of the fault analysis and the interpreted stress axis during the Cambrian synsedimentary tectonic event.

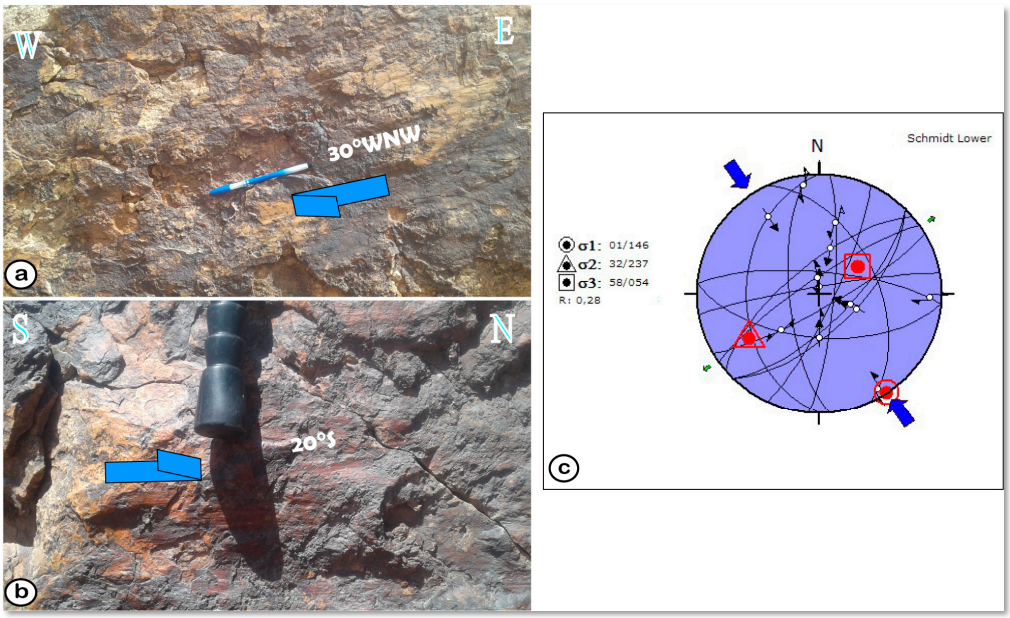

Figure 9. (**a**,**b**) Field photos show, respectively, a E-W dextral and N-S sinistral strike-slip faults; (**c**) stereographic projection and stress axes during the NW-SE compression.

- The NNE-SSE compressive event in the southern High Atlas Mesozoic Cover (***Da***)

At the north of Imiter mine, the infracenomanian red formation (sandstone, siltstone and mudstone) and Cenomanian-Turonian limestones were affected by multiple conju-

gate strike slip faults (Figure 11a,b). These NE-SW trending faults are sinistral with a small vertical component, and the NW-SE trending faults are dextral. The shape ratio $R = (\sigma2 - \sigma3)/(\sigma1 - \sigma3) = 0.5$ indicates that $\sigma2 \approx (\sigma1 + \sigma3)/2$ [82,83]. The stress tensors obtained from the kinematic data of these faults are consistent with a strike-slip regime. This tectonic state is characterized by a sub-vertical σ2 axis, a sub-horizontal ENE-WSW σ3 axis and a horizontal NNW-SSE trending σ1 axis (Figure 11c). This tectonic stage corresponds to the Atlas phase recorded from the Tinghir-Boumalne area [96,97].

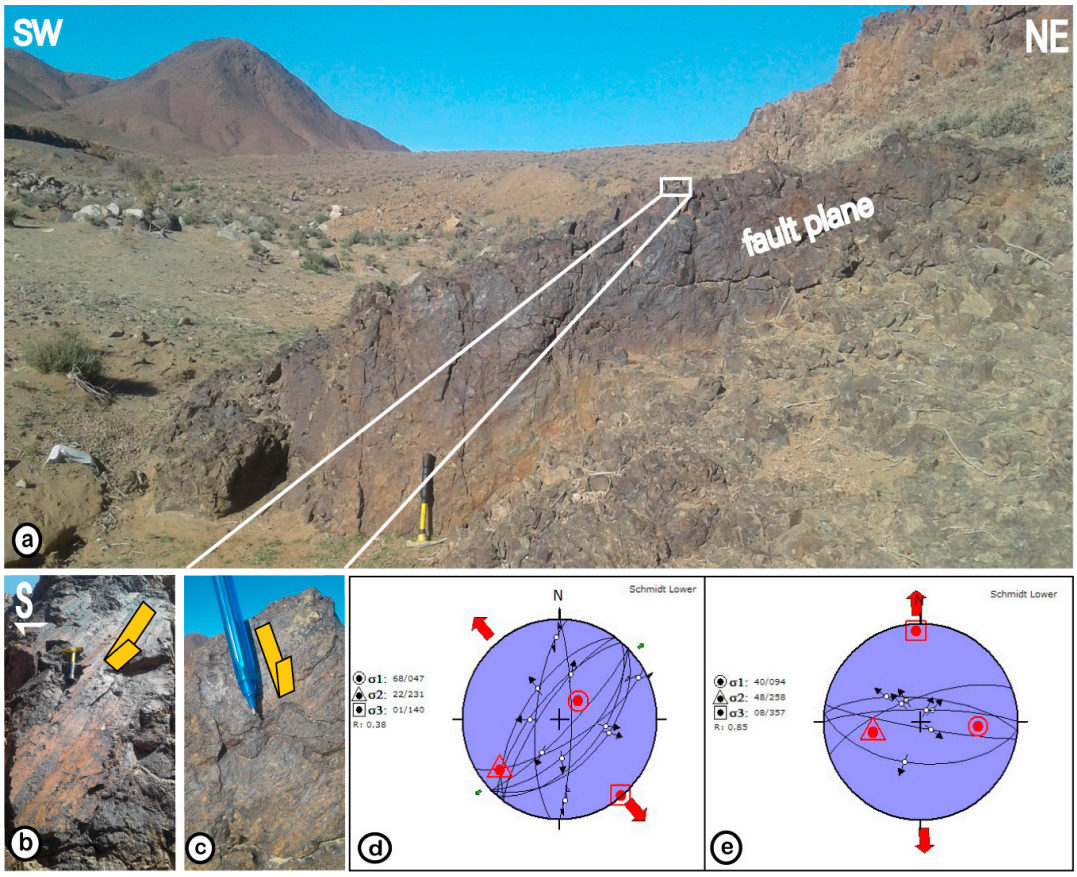

Figure 10. (**a**–**c**) Field photos shows a normal fault; (**d**,**e**) stereograms and stress axes orientation during the NW-SE extensional stage responsible for the Imiter fault collapse.

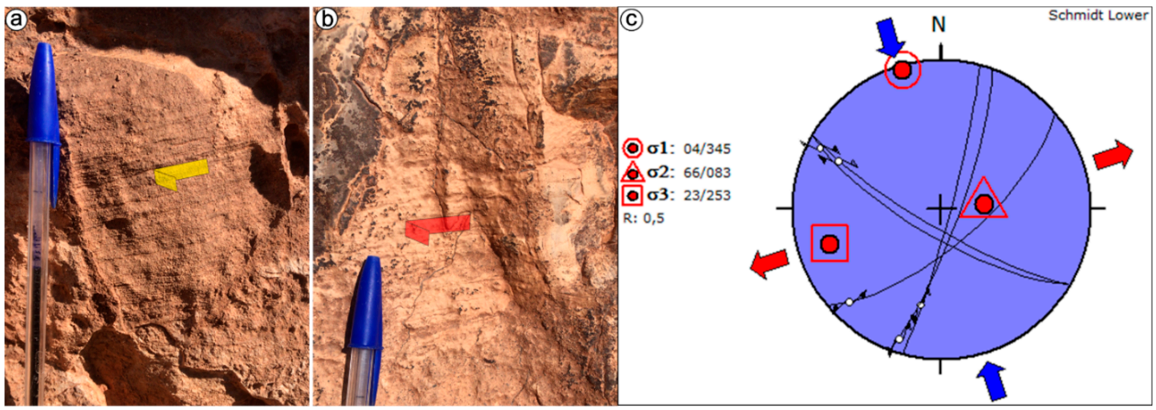

Figure 11. (**a**,**b**) Photographs of strike-slip faults affecting Cenomano-Turonian limestones north of Imiter mine; (**c**) stereogram and stress axes orientation during the Atlasic compression.

5. Discussion

The Imiter area on the northeastern side of the Saghro massif contains a variety of geological units, including the Cryogenian-late Ediacaran basement, represented by the "flysch-like" Saghro Group, the volcano-sedimentary units of the early Ediacaran Ouarzazate Group and the late Paleozoic sedimentary deposits. The Eastern Anti-Atlas area is affected by thick-skinned tectonic style [71,98,99], characterized by repeated remobilizations of basement faults during superimposed orogenic cycles in Pan-African-Cadomian, Variscan, and Alpine orogenies [100]. The structural analysis, documented in different geological formations, including basement rocks, allows the generation of a structural dataset, illustrating multiphase deformation of at least eight consecutive tectonic events affecting the eastern Saghro massif (Figure 12).

Orogenic event	Notation	Deformation age		Fault system	Stress state
Atlasic	Da	Neogene		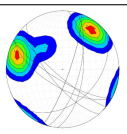	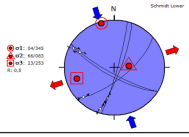
	Dt	Triassic		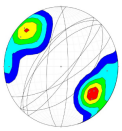	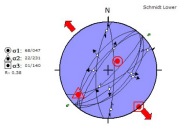
Variscan	Dv	Carboniferous-Permian		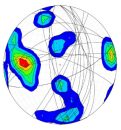	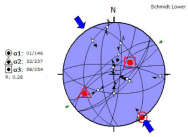
Late- Pan African-Cadomian	Dc	Cambrian		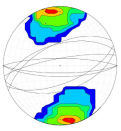	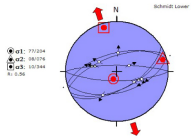
	Dp4	Ediacaran	upper	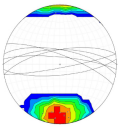	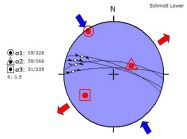
	Dp3			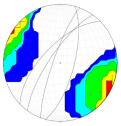	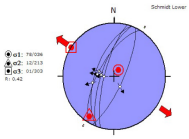
	Dp2		lower	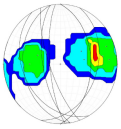	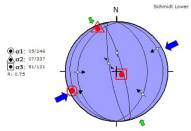
	Dp1			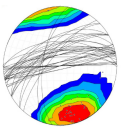	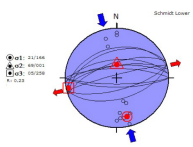

Figure 12. Comprehensive figure of fault system and paleostress evolution of major orogen affecting the Imiter area.

5.1. Late Pan-African-Cadomian Tectonic Events

5.1.1. Late Ediacaran Tectonic Events in the Saghro Group

As noted above, the Imiter inlier basement formed from "flysch-like" metasediments of the Saghro Group is affected by a pervasive northeast foliation, locally axial plane to northeast dipping folds (Dp1). This synmetamorphic deformation was previously assigned to the well-known regional Cryogenian Pan-African deformation along the central Anti-Atlas suture [17,68,76]. Among other thing, this assignment is based on the imprecise ages of the various Imiter plutons traversing the Imiter Saghro Group (K/Ar method, [101]. Recent geological studies dedicated to the Imiter area reveal precise ages of the associated igneous rocks and discuss the tectonic setting of the Saghro Group [25,26,71,79]. First, most of the Imiter granitoids (Igoudrane, Bou Teglimt, . . .) are younger than previously reported, as indicated by late Ediacaran age using the "zircon U–Pb" method [26,71,79]. On the other hand, the Saghro Group has a maximum depositional age of about 620–610 Ma based on detrital zircon geochronology [26,73,74]. Therefore, the depositional time of Saghro Group may have lasted from the Cryogenian to the end of the early Ediacaran. The NNE–trend deformation associated with low-grade greenschist metamorphism occurred before the emplacement of the late Ediacaran Ouarzazate Group, and thus later than the major Pan-African event documented along the Bou Azzer-Siroua Neoproterozoic suture (760–640 Ma) [28,48]. Saghro fold belt records (610–580 Ma) correspond to the latest compressional and/or transpressional, synmetamorphic event of the Pan-African-Cadomian orogenic cycle in the Saghro massif in eastern Anti-Atlas [24–26,28].

Following basement deformation, the proposed structural analysis allows the detection of an NW-SE to NS reverse faults with a strike-slip component, compatible with the ENE-WSW compression event (Dp2). Since this brittle event specifically affects the basement rather than the overlaying volcano-sedimentary Ouarzazate Group, it should be considered to belong to the final stage of the Saghro Group deformation, possibly during its exhumation before 580 Ma [25].

5.1.2. Late Ediacaran Tectonic Events in the Ouarzazate Group

Measurements of faults affecting the Ouarzazate Group formations in the Imiter area indicate that at least its lower units were affected by synsdepositional normal faults associated with the WNW-ESE extensional event (Dp3). In fact, at the Anti-Atlas scale, it is generally accepted that the Ouarzazate Group volcanoclastic sediments are characterized by marked and abrupt changes in thickness, indicating contributions to synsedimentary faults in creating horst and graben architecture [19,24,27,77,100,102–104]. These faults were inherited from ancient Pan-African faults and were subsequently reactivated as normal faults controlling the Ouarzazate Group deposits, possibly as hydrothermal drains to the Imiter Ag-Hg deposits [17,21].

Later, the Cryogenian basement and Ediacaran volcanoclastic deposits in the Imiter area were segmented by E-W oriented dextral strike-slip fault with smaller reverse components, consistent with an NNW-SSE compression event that precedes the deposition of the late middle Cambrian units (Dp4). Thus, a distinct unconformity marks the transition between the late Ediacaran and middle Cambrian sediments in the region. In addition, Ediacaran volcanic pebbles are found in the late conglomerate layers of the middle Cambrian "brèche à Micmacca". Most likely, this compression event may have been associated with prolonged exhumation and erosion of Ediacaran units. Therefore, this tectonic event is thought to represent the ultimate impetus for the Pan-African-Cadomian compressions in this area.

Elsewhere in the Anti-Atlas, the first Cambrian sediments cover para-conformably the Ouarzazate Group in the western and southwestern Anti-Atlas [103,104], or with more or less obvious angular unconformity in the central and eastern Anti-Atlas [24,100]. The geodynamic setting of the late Ediacaran Ouarzazate Group remains under debate in the context of the waning stages of the Pan-African-Cadomian orogeny. Global deposition in an extensional/transpressional tectonic regime is now allowed. Long-lived volcanoclastic

deposits of Ouarzazate Group (580–454 Ma) may have been interrupted by reported internal compression events in the western Saghro massif [24]. The angular unconformity described in the Precambrian-Cambrian boundary, mainly towards the northern Anti-Atlas areas, may correspond to a significant transpressional event that can be considered the last tectonic motion of the Pan-African-Cadomian orogeny.

5.1.3. Cambrian Extensional Events

In the Imiter area, Paleozoic deposition began with the middle Cambrian sediments, which still retain the synsedimentary ENE-WSW oriented normal faults, compatible with the NNW-SSE extensional event (Dc). Elsewhere, the Cambrian transgression developed from west to east in the Anti-Atlas [51]. In the western Anti-Atlas, the role of extensional tectonics in the early Cambrian rift is emphasized by the creation of relatively depressed areas first occupied by rivers and lakes in the late Neoproterozoic, then gradually invaded by a transgressive sea in the Cambrian [104,105]. The early Cambrian rifting ended at the end of the early Cambrian [106,107]. In the eastern Anti-Atlas, this extensional event continued into the middle Cambrian, with massive mafic volcanic activity south of the Ougnat massif [108].

5.2. Variscan Tectonic Events

Structural analysis of the fault network performed in the middle Cambrian sequences allowed the identification of three fault families: the NE-SW oriented reverse faults, the E-W oriented dextral faults, and the N-S oriented sinistral faults (Dv). This fault kinematics are compatible with the post-Cambrian NW-SE transpressional event. A dextral transpression event has been reported within the Paleozoic cover of the NE edge of the Saghro inlier [31,96]. In fact, the Paleozoic sequences north of the Imiter area are intersected by E-W-trending dextral faults associated with late Carboniferous transpressional deformation [30,31,96]. These structures show the autochthonous distribution of the Paleozoic rocks and the thin-skinned tectonic pattern of the Variscan deformation in the northern Imiter. The Imiter-Tineghir domain belongs to the Sub-Meseta zone belt, including also Skoura and Tamlelt regions [32] where the Variscan deformation shows a combination of dextral faulting and southward thrusting at the boundary of the West African Craton [30,31,109,110].

5.3. Atlasic-Alpine Tectonic Events

5.3.1. The Pre-Atlasic Triassic Crustal Extension and the Collapse of the Imiter Fault

In the Imiter area, many ENE-WSW to E-W faults, including the large Imiter and the related faults, show normal, vertical, or strike-slip displacement in response to the NNW-SSW transtensional tectonic regime (Dt). This event coincided with the Triassic-Early Jurassic rift peaking around 200 Ma, when the Anti-Atlas zone represented the uplift shoulder of the High Atlas rift [111,112]. Except for the intrusion of several NE-trending dykes and associated gabbro and dolerite sills [113,114], the Triassic sediments and associated basalts of the CAMP were completely eroded on the Anti-Atlas domain, probably during the Jurassic-Cretaceous periods of exhumation [58]. In addition to the intrusion of dolerite dykes and sills, many normal faults inherited from the Variscan faults affected the Paleozoic cover series, mainly in the eastern Anti-Atlas [57].

Finally, it is worth noting that the tectono-thermal effect of the Late Triassic extensional event on the Anti-Atlas crust may be greater than previously thought. This tectono-volcanic event, accompanied by shallow magmatic emplacement and hydrothermal fluid circulation, may have had a direct impact on the formation or redeposition of precious metals, including the Imiter silver deposit.

5.3.2. The NNE-SSE Compressive Event in the Southern High Atlas Mesozoic Cover

Because of its location near the southern part of the Cenozoic High Atlas chain, fault measurements were performed in the southern sub-Atlas cover to assess the tectonic impact of Cenozoic shortening. Here, the infracenomanian red beds and the Cenomanian-Turonian

limestones are affected by NW-SE oriented dextral strike-slip faults and NE-SW oriented sinistral strike-slip faults, consistent with the NNW-SSE Atlas compression (Da). Similar tectonic events have also been recorded in the Tinghir-Boumalne area [96,97].

6. Discussion of the Structural Framework Imiter Silver Deposit

East of Saghro massif is known for the world-class Imiter silver deposit, hosted by the turbidites of the early Ediacaran Saghro Group and the overlying the late Ediacaran volcanoclastic Ouarzazate Group [18]. The Ouarzazate Group is characterized by ash-flow caldera emplacement, thick and widespread ignimbrites, lava, and pyroclastic sedimentary rocks, interspersed with extensive magmatism between 575 and 555 Ma. In this regard, several authors agree on the genetic link between Imiter silver mineralization and late Ediacaran magmatism, mainly felsic volcanism, dating to 550 ± 3 Ma [19,21,77].

Given the economic importance of the Imiter deposit, a number of structural studies have been completed in and around the mine, where silver mineralization is roughly located on the large EW fault network and its N60 to N70 relays. First structural studies [17,18] revealed the existence of two major tectonic events, the first associated with an NNW-SSE to NS extensional tectonic event, and the second controlled by sinistral strike-slip faults. Ref. [21] developed a three-stage model including a major phase of NW-SE to WNW-ESE shortening, responsible for the ENE to NE dextral transpressive relays, associated with the essential of the Imiter mercury-silver mineralization and acidic volcanic-plutonic manifestations. In the second phase, the previous shear band reopens under NS shortening with a sinistral shear with a normal component, followed by an altered phase favoring local Ag enrichment.

This work highlights several tectonic phases that affect the Imiter area. The main NW-SE to WNW-ESE shortening of [21] which accounts for the essential of the Imiter silver mineralization appears to be compatible with the dextral faults cutting the volcanic and crystalline basement described in this study. Therefore, faults associated with this phase are associated with the NNW-SSE compression phase (Dp4) which is considered to be late Ediacaran. Although these structures were reactivated in the second stage, the major sinistral shear-zones with a normal component, was of no economic significance. It is assumed that it is a rather recent tectonic event and could correspond to the extensive NNW-SSE Cambrian (Dc) phase described in this study that formed syn-sedimentary faults in the Cambrian strata. The last stage of alteration that may have resulted in localized concentrations of Ag mineralization can be locked for in later thermal events; the Late Triassic NNW-SSE transtensional tectonic regime (Dt) during the Pangea breakup, with NE-trending CAMP dykes can be considered a possible reconcentration event of Imiter Silver deposit.

7. Conclusions

A structural analysis of various geological rocks in the northeastern part of the Saghro massif in the east Anti-Atlas was carried out on site measurements. Different structures are distinguished, their tectonic stress direction and their effects on various geological units elucidated. The obtained results underscore the multistage tectonic regimes spanning at least eight tectonic episodes, including the late Pan-African-Cadomian, Variscan, and the Atlasic orogenesis.

- During the late Pan-African-Cadomian event, the Cryogenian-late Ediacaran Saghro Group underwent low-grade metamorphic deformation, resulting in multiscale folding, with the axial plane represented by pervasive ENE-WSW foliation (Dp1). The brittle ENE-WSW compression event coincided with the exhumation of the Saghro Group basement before to the early Ediacaran (Dp2). The Saghro Group basement was structured during the compressional and/or transpressional late Pan-African-Cadomian events (600–580 Ma).

- The unconformably overlying deposition of the early Ediacaran Ouarzazate Group occurred in a WNW-ESE extensional environment (Dp3), followed by a NNW-SSE compression event (Dp4). This may have occurred later during the regional exhumation and erosion of the eastern Anti-Atlas.
- The middle Cambrian deposits are the oldest Paleozoic sediments in this area and are governed by a synsedimentary ENE-WSW normal faults compatible with the NNW-SSE extensional event (Dc).
- During the late Carboniferous, Variscan shortening was recorded by NW-SE transpression event, responsible for a combined dextral south thrusting faults (Dv) in the Sub-Mesetian zone of Morocco.
- Mesozoic evolution began with the Late Triassic NNW-SSE transtensional tectonic regime (Dt), with NE-trending CAMP dykes during the Pangea breakup. Finally, the last exhumation of this area was during the NNW-SSE Atlas shortening (Da), which is responsible for the High Atlas Mountains uplift.

The current elucidation of tectonic structures and associated stress directions, and their impact on various geological units, is critical to understanding the relationship between structures and silver ore deposits in the Imiter districts and further beyond the eastern Anti-Atlas belt.

Author Contributions: Conceptualization, Y.A. and A.S.; methodology, Y.A.; software, Y.A. and D.Y.; validation, A.S., N.Y. and D.Y.; formal analysis, Y.A.; resources, A.A.L.; data curation, D.Y.; writing—original draft preparation, Y.A., A.S., and A.B.P.; writing—review and editing, A.S., A.B.P. and M.H.; visualization, A.B.P.; supervision, A.S., N.Y., and A.B.P.; project administration, Y.A. All authors have read and agreed to the published version of the manuscript.

Funding: This research received no external funding.

Data Availability Statement: Not applicable.

Acknowledgments: This work is a part Youssef Atif's doctoral dissertation which be submitted to the Department of Geology, Faculty of Sciences Semlalia, Cadi Ayyad University of Marrakech. This is the result of a collaboration between DLGR Laboratory and Imiter Mine.

Conflicts of Interest: The authors declare no conflict of interest.

References

1. Zhou, Y.; Xu, D.; Dong, G.; Chi, G.; Deng, T.; Cai, J.; Ning, J.; Wang, Z. The role of structural reactivation for gold mineralization in northeastern Hunan Province, South China. *J. Struct. Geol.* **2021**, *145*, 104–306. [CrossRef]
2. Santosh, M.; Groves, D.I. Global metallogeny in relation to secular evolution of the Earth and supercontinent cycles. *Gondwana Res.* **2022**, *107*, 395–422. [CrossRef]
3. Kwak, Y.; Park, S.-I.; Park, C. Structural controls on crustal fluid redistribution and hydrothermal gold deposits: A review on the suction pump and fault valve models. *Korea Econ. Environ. Geol.* **2022**, *55*, 183–195. [CrossRef]
4. Shirazi, A.; Hezarkhani, A.; Pour, A.B. Fusion of lineament factor (Lf) map analysis and multifractal technique for massive sulfide copper exploration: The Sahlabad area, East Iran. *Minerals* **2022**, *12*, 549. [CrossRef]
5. Brogi, A.; Fulignati, P. Tectonic control on hydrothermal circulation and fluid evolution in the Pietratonda–Poggio Peloso (southern Tuscany, Italy) carbonate-hosted Sb-mineralization. *Ore Geol. Rev.* **2012**, 158–171. [CrossRef]
6. Vezzoni, S.; Dini, A.; Rocchi, S. Reverse telescoping in a distal skarn system (Campiglia Marittima, Italy). *Ore Geol. Rev.* **2016**, *77*, 176–193. [CrossRef]
7. Zucchi, M.; Brogi, A.; Liotta, D.; Caggianelli, A.; Dini, A.; Ventruti, G.; Ruggeri, G.; Matera, P. Fractures, fluid flow and inherited structures in geothermal systems-inputs from the Fe-Ore deposits of eastern Elba island (northern Apennines, Italy). *Geol. Mag.* **2022**, 1–14. [CrossRef]
8. Bernardinetti, S.; Pieruccioni, D.; Mugnaioli, E.; Talarico, F.M.; Trotta, M.; Harroud, A.; Tufarolo, E. A pilot study to test the reliability of the ERT method in the identification of mixed sulphides bearing dykes: The example of Sidi Flah mine (Anti-Atlas, Morocco). *Ore Geol. Rev.* **2018**, *101*, 819–838. [CrossRef]
9. Funedda, A.; Naitza, S.; Buttau, C.; Cocco, F.; Dini, A. Structural controls of ore mineralization in a polydeformed basement: Field examples from the Variscan Baccu Locci shear zone (SE Sardinia, Italy). *Minerals* **2018**, *8*, 456. [CrossRef]
10. Abd El-Wahed, M.A.; Zoheir, B.; Pour, A.B.; Kamh, S. Shear-Related Gold Ores in the Wadi Hodein Shear Belt, South Eastern Desert of Egypt: Analysis of Remote Sensing, Field and Structural Data. *Minerals* **2021**, *11*, 474. [CrossRef]

11. Cocco, F.; Attardi, A.; Deidda, M.L.; Fancello, D.; Funedda, A.; Naitza, S. Passive Structural Control on Skarn Mineralization Localization: A Case Study from the Variscan Rosas Shear Zone (SW Sardinia, Italy). *Minerals* **2022**, *12*, 272. [CrossRef]
12. Xie, Y.; Gao, H.; Kong, H.; Zheng, H. Structural Controls on Mineralization within the Huanggou Gold Deposit in the Southern Mesozoic Xuefengshan Orogen, South China. *Minerals* **2022**, *12*, 751. [CrossRef]
13. Zoheir, B.; El-Wahed, M.A.; Pour, A.B.; Abdelnasser, A. Orogenic gold in transpression and transtension zones: Field and remote sensing studies of the Barramiya–Mueilha sector, Egypt. *Remote Sens.* **2019**, *11*, 2122. [CrossRef]
14. Zoheir, B.; Emam, A.; Abd El-Wahed, M.; Soliman, N. Gold endowment in the evolution of the Allaqi-Heiani suture, Egypt: A synthesis of geological, structural, and space-borne imagery data. *Ore Geol. Rev.* **2019**, *110*, 102938. [CrossRef]
15. Zoheir, B.; Emam, A.; Abdel-Wahed, M.; Soliman, N. Multispectral and radar data for the setting of gold mineralization in the south eastern desert, Egypt. *Remote Sens.* **2019**, *11*, 1450. [CrossRef]
16. Hindermeyer, J.; Gauthier, H.; Destombes, J.; Choubert, G.; Faure-Muret, A. Carte géologique du Maroc, Jbel Saghro-Dadès (Haut Atlas central, sillon sud-atlasique et Anti-Atlas oriental)—Echelle 1/200.000. In *Notes et Mémoires*; Editions du Service Géologique du Maroc: Rabat, Morocco, 1977; p. 161.
17. Ouguir, H.; Macaudière, J.; Dagallier, G.; Qadrouci, A.; Leistel, J. Cadre structural du gite Ag-Hg d'Imiter (Anti Atlas, Maroc) implication métallogénique (structural framework of the Ag-Hg deposit of imiter (Anti-Atlas, Morocco); metallogenic inferences). *Bull. Soc. Géol. Fr.* **1994**, *165*, 233–248. [CrossRef]
18. Levresse, G. Contribution à l'établissement d'un mode génétique des gisements d'Imiter (Ag-Hg), Bou Madine (Pb-Zn-Cu-Ag-Au) et Bou Azzer (Co-Ni-As-Au-Ag) dans l'Anti-Atlas Marocain. Ph.D. Thesis, Institut National Polytechnique de Lorraine (INPL), Nancy, France, 2001.
19. Cheilletz, A.; Levresse, G.; Gasquet, D.; Azizi-Samir, M.; Zyadi, R.; Archibald, D.A.; Farrar, E. The giant Imiter silver deposit: Neoproterozoic epithermal mineralization in the Anti-Atlas, Morocco. *Miner. Depos.* **2002**, *37*, 772–781. [CrossRef]
20. Thomas, R.J.; Fekkak, A.; Ennih, N.; Errami, E.; Loughlin, S.C.; Gresse, P.G.; Chevallier, L.P.; Liégeois, J.P. A new lithostratigraphic framework for the Anti-Atlas orogen, Morocco. *J. Afr. Earth Sci.* **2004**, *39*, 217–226. [CrossRef]
21. Tuduri, J.; Chauvet, A.; Ennaciri, A.; Mod, L.B. Modéle de formation du gisement d'argent d'Imiter (Anti-Atlas oriental, Maroc). Nouveaux apports de l'analyse structurale et minéralogique. *Comptes Rendus Géosci. Elsevier Masson* **2006**, *338*, 253–261. Available online: https://hal-insu.archives-ouvertes.fr/hal-00023638 (accessed on 1 January 2022). [CrossRef]
22. Gasquet, D.; Levresse, G.; Cheilletz, A.; Azizi-samir, M.R.; Mouttaqi, A. Contribution to a geodynamic reconstruction of the Anti-Atlas (Morocco) during pan-african times with the emphasis on inversion tectonics and metallogenic activity at the Precambrian—Cambrian transition. *Precambian Res.* **2005**, *140*, 157–182. [CrossRef]
23. Continental evolution: The geology of Morocco. In *Lecture Notes in Earth Sciences*; Michard, A.; Saddiqi, O.; Chalouan, A.; Frizon de Lamotte, D., Eds.; Springer: Berlin, Germany, 2008; Volume 116, pp. 1–31. [CrossRef]
24. Walsh, G.J.; Benziane, F.; Aleinikoff, J.N.; Harrison, R.W.; Yazidi, A.; Burton, W.C.; Quick, J.E.; Saadane, A. Neoproterozoic tectonic evolution of the jebel Saghro and Bou Azzer-El Graara inliers, eastern and central Anti-Atlas, Morocco. *Precambrian Res.* **2012**, *216–219*, 23–62. [CrossRef]
25. Michard, A.; Soulaimani, A.; Ouanaimi, H.; Raddi, Y.; Aït Brahim, L.; Rjimati, E.C.; Baidder, L.; Saddiqi, O. Saghro group in the Ougnat massif (Morocco), an evidence for a continuous cadomian basin along the northern west african craton. *Comptes Rendus-Geosci.* **2017**, *349*, 81–90. [CrossRef]
26. Errami, E.; Linnemann, U.; Hofmann, M.; Gärtner, A.; Zieger, J.; Gärtner, J.; Mende, K.; El Kabouri, J.; Gasquet, G.; Ennih, N. From panafrican transpression to cadomian transtension at the west african margin: New U-Pb zircon ages from the eastern Saghro inlier (Anti-Atlas, Morocco). *Geol. Soc. Lond. Spec. Publ.* **2020**, *503*, 209–233. [CrossRef]
27. Thomas, R.J.; Chevallier, L.P.; Gresse, P.G.; Harmer, R.E.; Eglington, B.M.; Armstrong, R.A.; De Beer, C.H.; Martini, J.E.J.; De Kock, G.S.; Macey, P.H.; et al. Precambrian evolution of the Sirwa window, Anti-Atlas orogen, Morocco. *Precambrian Res.* **2002**, *118*, 1–57. [CrossRef]
28. Hefferan, K.; Soulaimani, A.; Samson, S.D.; Admou, H.; Inglis, J.; Saquaque, A.; Latifa, C.; Heywood, N. A reconsideration of panafrican orogenic cycle in the Anti-Atlas mountains, Morocco. *J. Afr. Earth Sci.* **2014**, *98*, 34–46. [CrossRef]
29. Soulaimani, A.; Ouanaimi, H.; Saddiqi, O. The anti-Atlas panafrican belt (Morocco): Overview and pending questions. *Comptes rendus-Geosci.* **2018**, *350*, 279–288. [CrossRef]
30. Michard, A.; Yazidi, A.; Benziane, F.; Hollard, H.; Willefet, S. Foreland thrusts and olistostromes on the pre-sahara margin of the Variscan orogen, Morocco. *Geology* **1982**, *10*, 253–256. [CrossRef]
31. Cerrina Feroni, A.; Ellero, A.; Malusà, M. Transpressional tectonics and nappe stacking along the southern Variscan front of Morocco. *Int. J. Earth Sci.* **2010**, *99*, 1111–1122. [CrossRef]
32. Michard, A.; Ouanaimi, H.; Hoepffner, C.; Soulaimani, A.; Baidder, L. Comment on tectonic relationships of southwest iberia with the allochthons of northwest iberia and the Moroccan variscides by J.F. Simancas et al. [C. R. Geoscience 341 (2009) 103-113]. *Comptes Rendus-Geosci.* **2010**, *342*, 170–174. [CrossRef]
33. Choubert, G. Histoire géologique du Précambrien de l'Anti-Atlas. *Notes Et Mémoires Du Serv. Géologique Du Maroc* **1963**, *162*, 352.
34. Ait Malek, H.; Gasquet, D.; Bertand, J.M.L.J. Géochronologie U-Pb sur zircon de granitoides éburnéens et panafricains dans les boutonnières protérozoiques d'Igherm, du Kerdous et du Ba Draa (Anti-Atlas occidental, Maroc). *Comptes Rendus Acad. Des Sci.* **1998**, *327*, 819–826. [CrossRef]

35. Walsh, G.J.; Aleinikoff, J.N.; Benziane, F.; Yazidi, A.; Armstrong, T.R. U-Pb zircon geochronology of the paleoproterozoic tagragra de Tata inlier and its Neoproterozoic cover, western Anti-Atlas, Morocco. *Precambrian Res.* **2002**, *117*, 1–20. [CrossRef]
36. Gasquet, D.; Chevremont, P.; Baudin, T.; Chalot-prat, F.; Guerrot, C. Polycyclic magmatism in the tagragra d'Akka and Kerdous—Tafeltast inliers (western Anti-Atlas, Morocco). *J. Afr. Earth Sci.* **2004**, *39*, 267–275. [CrossRef]
37. Blein, O.; Baudin, T.; Chèvremont, P.; Soulaimani, A.; Admou, H.; Gasquet, P.; Cocherie, A.; Egal, E.; Youbi, N.; Razin, P.; et al. Geochronological constraints on the polycyclic magmatism in the Bou Azzer-El Graara inlier (central Anti-Atlas Morocco). *J. Afr. Earth Sci.* **2014**, *99*, 287–306. [CrossRef]
38. Blein, O.; Chevremont, P.; Baudin, T.; Hafid, A.; Admou, H.; Soulaimani, A.; Ouanaimi, H.; Bouabdelli, M.; Gasquet, D.; Maxime, P. Contrasting paleoproterozoic granitoids in the Kerdous, tagragra d'Akka, Agadir-Melloul and Iguerda inliers (western Anti-Atlas, Morocco). *J. Afr. Earth Sci.* **2022**, *189*, 104500. [CrossRef]
39. Kouyate, D.; Soderlund, U.; Youbi, N.; Ernst, R.; Hafid, A.; Ikenne, M.; Soulaimani, A.; Bertrand, H.; El Janati, M.; Rakha Chaham, K. U-Pb baddeleyite ages of 2040 Ma, 1650 Ma and 885 Ma on dolerites in the west african craton (Anti-Atlas Inliers): Possible links to break-up of precambrian supercontinents. *Lithos* **2012**, *174*, 71–84. [CrossRef]
40. Baidada, B.; Cousens, B.; Alansari, A.; Soulaimani, A.; Barbey, P.; Ilmen, S.; Ikenne, M. Geochemistry and Sm–Nd isotopic composition of the Imiter panafrican granitoids (Saghro massif, eastern Anti-Atlas, Morocco): Geotectonic implications. *J. Afr. Earth Sci.* **2017**, *127*, 99–112. [CrossRef]
41. Ait Lahna, A.; Tassinari, C.C.G.; Youbi, N.; Admou, H.; Bouougri, E.H.; Chaib, L.; Ernst, R.E.; Soderlund, U.; Boumehdi, A.; Bensalah, M.K.; et al. Refining the stratigraphy of the taghdout group by using the U–Pb geochronology of the taghdout sill (Zenaga inlier, Anti-Atlas, Morocco). *Acta Geol. Sin.* **2016**, *90*, 1. [CrossRef]
42. El Bahat, A.; Ikenne, M.; Söderlund, U.; Cousens, B.; Youbi, N.; Ernst, R.; Soulaimani, A.; El Janati, M.; Hafid, A. U-Pb baddeleyite ages and geochemistry of dolerite dykes in the Bas Drâa inlier of the Anti-Atlas of Morocco: Newly identified 1380Ma event in the west african craton. *Lithos* **2013**, *174*, 85–98. [CrossRef]
43. Youbi, N.; Kouyaté, D.; Soderlund, U.; Ernst, R.E.; Soulaimani, A.; Hafid, A.; Ikenne, M.; El Bahat, A.; Bertrand, H.; Chaham, K.R.; et al. The 1750 Ma magmatic event of the west african craton (Anti-Atlas, Morocco). *Precambrian Res.* **2013**, *236*, 106–123. [CrossRef]
44. Leblanc, M. *Ophiolites Précambriennes et Gîtes Arséniés de Cobalt (Bou-Azzer, 572 Maroc)*; Centre Geologique et Geophysique: Montpellier, France, 1975.
45. Bouougri, E.H.; Saquaque, A. Lithostratigraphic framework and correlation of the Neoproterozoic northern west african craton passive margin sequence (Siroua-Zenaga-Bouazzer Elgraara inliers, central Anti-Atlas, Morocco): An Integrated Approach. *J. Afr. Earth Sci.* **2004**, *39*, 227–238. [CrossRef]
46. Leblanc, M.; Lancelot, J.R. Interpretation geodynamique du domaine panafricain (Precambrien terminal) de l'anti-Atlas (Maroc) a partir de donnees geologiques et geochronologiques. *Can. J. Earth Sci.* **1980**, *17*, 142–155. [CrossRef]
47. Hodel, F.; Triantafyllou, A.; Berger, J.; Macouin, M.; Baele, J.M.; Mattielli, N.; Monnier, C.; Trindade, R.I.F.; Ducea, M.N.; Chatir, A.; et al. The Moroccan Anti-Atlas ophiolites: Timing and melting processes in an intra-oceanic arc-back-arc environment. *Gondwana Res.* **2020**, *86*, 182–202. [CrossRef]
48. Triantafyllou, A.; Berger, J.; Baele, J.M.; Diot, H.; Ennih, N.; Plissart, G.; Monnier, C.; Watlet, A.; Bruguier, O.; Spagna, P.; et al. The Tachakoucht-Iriri-Tourtit arc complex (Moroccan Anti-Atlas): Neoproterozoic records of polyphased subduction-accretion dynamics during the panafrican orogeny. *J. Geodyn.* **2016**, *96*, 81–103. [CrossRef]
49. Triantafyllou, A.; Berger, J.; Baele, J.; Bruguier, O.; Diot, H.; Ennih, N.; Monnier, C.; Plissart, G.; Vandycke, S.; Watlet, A. Intra-oceanic arc growth driven by magmatic and tectonic processes recorded in the Neoproterozoic Bougmane arc complex (Anti-Atlas, Morocco). *Precambrian Res.* **2018**, *304*, 39–63. [CrossRef]
50. El Boukhari, A.; Chaabane, A.; Rocci, G.; Tane, J. Upper proterozoic ophiolites of the siroua massif (Anti-Atlas, Morocco) a marginal sea and transform fault system. *J. Afr. Earth Sci.* **1992**, *14*, 67–80. [CrossRef]
51. Benziane, F.; Prost, A.; Yazidi, A. Le passage du précambrien au cambrien précoce volcanique et sédimentaire de l'Anti-Atlas oriental ; comparaison avec l'Anti-Atlas occidental. *Bull. Soc. Geol. Fr.* **1983**, *25*, 549–556. [CrossRef]
52. Landing, E.; Bowring, S.A.; Davidek, K.L.; Westrop, S.R.; Geyer, G.; Heldmaier, W. Duration of the early cambrian: U–Pb ages of volcanic ashes from avalon and gondwana. *Can. J. Earth Sci.* **1998**, *35*, 329–338. [CrossRef]
53. Maloof, A.C.; Schrag, D.P.; Crowley, J.L.; Bowring, S.A. An expanded record of early cambrian carbon cycling from the Anti-Atlas margin, Morocco. *Can. J. Earth Sci.* **2005**, *42*, 2195–2216. [CrossRef]
54. Burkhard, M.; Caritg, S.; Helg, U.; Robert-charrue, C. Tectonics of the Anti-Atlas of Morocco. *Comptes Rendus Geosci.* **2006**, *338*, 11–24. [CrossRef]
55. Soulaimani, A.; Le Corre, C.; Frazdaq, R. Déformation hercynienne et relation socle / couverture dans le domaine du Bas-Drâa (Anti-Atlas occidental, Maroc). *J. Afr. Earth Sci.* **1997**, *24*, 271–284. [CrossRef]
56. Caritg, S.; Burkhard, M.; Ducommun, R.; Helg, U.; Kopp, L.; Sue, C. Fold interference patterns in the late Palaeozoic Anti-Atlas belt of Morocco. *Terra Nova* **2004**, *16*, 27–37. [CrossRef]
57. Robert-Charrue, C.; Burkhard, M. Inversion tectonics, interference pattern and extensional fault-related folding in the eastern Anti-Atlas, Morocco. *Swiss J. Geosci.* **2008**, *101*, 397–408. [CrossRef]
58. Malusà, M.G.; Polino, R.; Feroni, A.C.; Ellero, A.; Ottria, G.; Baidder, L.; Musumeci, G. Post-Variscan tectonics in eastern Anti-Atlas (Morocco). *Terra Nova* **2007**, *19*, 481–489. [CrossRef]

59. Gouiza, M.; Hall, J.; Welford, J.K. Tectono-stratigraphic evolution and crustal architecture of the orphan basin during north atlantic rifting. *Int. J. Earth Sci.* **2016**, *106*, 917–937. [CrossRef]
60. Oukassou, M.; Saddiqi, O.; Barbarand, J.; Sebti, S.; Baidder, L.; Michard, A. Post-Variscan exhumation of the central Anti-Atlas (Morocco) constrained by zircon and apatite fission-track thermo-chronology. *Terra Nova* **2013**, *25*, 151–159. [CrossRef]
61. Baidada, B.; Ikenne, M.; Barbey, P.; Soulaimani, A.; Cousens, B.; Haissen, F.; Ilmen, S.; Alansari, A. SHRIMP U–Pb zircon geochronology of the granitoids of the Imiter inlier: Constraints on the panafrican events in the Saghro massif, Anti-Atlas (Morocco). *J. Afr. Earth Sci.* **2019**, *150*, 700–810. [CrossRef]
62. Stone, B.D.; Benziane, F.; El Fahssi, A.; Yazidi, A.; Walsh, G.J.; Yazidi, M.; Saadane, A.; Ejjaouani, H.; Kalai, M. Carte géologique Au 1/50 000, seuille Sidi Flah. *Notes Et Mémoires Du Serv. Géologique Du Maroc* **2008**, *467*, 114.
63. Benziane, F.; Yazidi, A.; Saadane, A.; Yazidi, M.; El Fahssi, A.; Stone, B.D.; Walsh, G.J.; Burton, W.C.; Aleinikoff, J.N.; Ejjaouani, H.; et al. Carte géologique au 1/50 000, feuille Qal'at Mgouna. *Notes Et Mémoires Du Serv. Géologique Du Maroc* **2008**, *468*, 139.
64. Harrison, R.W.; Yazidi, A.; Benziane, F.; Quick, J.E.; El Fahssi, A.; Stone, B.D.; Yazidi, M.; Saadane, A.; Walsh, G.J.; Aleinikoff, J.N.; et al. Carte géologique Au 1/50 000, feuille Tizgui. *Notes Et Mémoires Du Serv. Géologique Du Maroc* **2008**, *470*, 131.
65. Walsh, G.J.; Benziane, F.; Burton, W.C.; El Fahssi, A.; Yazidi, A.; Yazidi, M.; Saadane, A.; Aleinikoff, J.N.; Ejjaouani, H.; Harrison, R.W.; et al. Carte géologique Au 1/50 000, feuille Bouskour. *Notes Et Mémoires Du Serv. Géologique Du Maroc* **2008**, *469*, 131.
66. Ouguir, H.; Macaudiere, J.; Dagallier, G. Le Protérozoïque supérieur d'Imiter, Saghro oriental, Maroc: Un contexte géodynamique d'arrière-arc. *J. Afr. Earth Sci.* **1996**, *22*, 173–189. [CrossRef]
67. Fekkak, A.; Pouclet, A.; Benharref, M. The middle Neoproterozoic Sidi Flah group (Anti-Atlas, Morocco): Synrift deposition in a panafrican continent/ocean transition zone. *J. Afr. Earth Sci.* **2003**, *37*, 73–87. [CrossRef]
68. Saquaque, B.A.L.I.; Benharref, M.; Abia, H.; Mrini, Z.; Reuber, I.; Karson, J.A. Evidence for a panafrican volcanic arc and wrench fault tectonics in the jbel Saghro, Anti-Atlas, Morocco. *Geol. Rundsch.* **1992**, *81*, 1–13. [CrossRef]
69. Fekkak, A.; Pouclet, A.; Ouguir, H.; Ouazzani, H.; Badra, L.; Gasquet, D. Géochimie et signification géotectonique des volcanites du gryogénien inférieur du Saghro (Anti-Atlas oriental, Maroc)/geochemistry and geotectonic significance of early cryogenian volcanics of Saghro (eastern Anti-Atlas, Morocco). *Geodin. Acta* **2001**, *14*, 373–385. [CrossRef]
70. Choubert, G. Coup d'œil sur la fin du Précambrien et le début du Cambrien dans le sud marocain. *Notes du Service Géologique du Maroc.* **1959**, *144*, 7–34.
71. Schiavo, A.; Taj-Eddine, K.; Algouti, A.; Benvenuti, M.; Dal Piaz, G.V.; Eddebbi, A.; El Boukhari, A.; Laftouhi, N.; Massironi, M.; Moratti, G.; et al. Carte géologique du Maroc au 1/50,000, Feuille Imiter. *Notes Et Mémoires Du Serv. Géologique Du Maroc* **2007**, *518*, 96.
72. Marini, F.; Ouguir, H. Un nouveau jalon dans l'histoire de la distension pré-panafricaine au Maroc : Le précambrien II des boutonnières du Jbel Saghro nord-oriental (Anti-Atlas, Maroc). *Comptes Rendus Acad. Sci. Paris.* **1990**, *310*, 577–582.
73. Liégeois, J.P.; Fekkak, A.; Bruguier, O.; Errami, E.; Ennih, N. The lower Ediacaran (630–610 Ma) Saghro Group: An orogenic transpressive basin development during the early metacratonic evolution of the Anti-Atlas (Morocco). Proceedings of the IGCP-485 4th Meeting. Abstract., Algiers, Algeria; 2006, Volumn 57. Available online: https://www.researchgate.net/publication/304014598 (accessed on 1 January 2022).
74. Abati, J.; Mohsine, A.; Gerdes, A.; Ennih, N. Detrital zircon ages of Neoproterozoic sequences of the Moroccan Anti-Atlas belt. *Precambrian Res.* **2010**, *181*, 115–128. [CrossRef]
75. Ait Lahna, A.; Youbi, N.; Tassinari, C.C.G.; Basei, M.A.S.; Ernst, R.E.; Chaib, L.; Barzouk, A.; Mata, J.; Gärtner, A.; Admou, H.; et al. Revised stratigraphic framework for the lower Anti-Atlas supergroup based on U–Pb geochronology of magmatic and detrital zircons (Zenaga and Bou Azzer-El Graara inliers, Anti-Atlas belt, Morocco). *J. Afr. Earth Sci.* **2020**, *171*, 103946. [CrossRef]
76. Ighid, L.; Saquaque, A.; Reuber, I. Plutons syn-cinématiques et la déformation panafricaine majeure dans le saghro oriental (boutonnière d'Imiter, Anti-Atlas, Maroc). *Comptes Rendus L'académie Des Sci. Paris.* **1989**, *309*, 615–620.
77. Levresse, G.; Cheilletz, A.; Gasquet, D.; Reisberg, L.; Deloule, E.; Marty, B.; Kyser, K. Osmium, sulphur, and helium isotopic results from the giant Neoproterozoic epithermal Imiter silver deposit, Morocco: Evidence for a mantle source. *Chem. Geol.* **2004**, *207*, 59–79. [CrossRef]
78. Ikenne, M.; Ennaciri, A.; Ouguir, H.; Cousens, B.; Ziyadi, R.; Mouhagir, M.; El-Gaouzi, A. Geochemical signature and geodynamic significance of an Ag-Hg mineralized dyke swarm in the neoproterozoic Ilier of Imiter-anti-atlas (morocco). *Ofioliti* **2007**, *32*, 109–118. [CrossRef]
79. Baidada, B.; Alansari, A.; Zoheir, B.; Ilmen, S.; Soulaimani, A.; Ikenne, M. Iron oxide copper-gold (IOCG) mineralization at the Imiter inlier, Eastern Anti-Atlas, Morocco. *Geochemistry* **2018**, *78*, 462–478. [CrossRef]
80. Massironi, M.; Moratti, G.; Algouti, A.; Benvenuti, M.; Dal Piaz, G.V.; Eddebbi, A.; El Boukhari, A.; Laftouhi, N.; Ouanaimi, H.; Schiavo, A.; et al. Carte géologique du maroc Au 1/50,000, feuille Boumalne. *Notes Mémoires Serv. Géologique Du Maroc* **2007**, *521*, 80.
81. Tuduri, J. Processus de formation et relations spatio-temporelles des minéralisations à or et argent en contexte volcanique Précambrien (Jbel Saghro, Anti Atlas, Maroc). Implications sur les relations déformations-magmatisme-volcanis,me-hydrothermalisme. Thèse, Université d'Orléans, France, 2005. Available online: https://tel.archives-ouvertes.fr/tel-00008937v3 (accessed on 30 November 2022).

82. Delvaux, D.; Moeys, R.; Stapel, G.; Petit, C.; Levi, K.; Miroshnichenko, A. Paleostress reconstructions and geodynamics of the Baikal region, Central Asia. Part II: Cenozoic rifting. *Tectonophys* **1997**, *282*, 1–38. [CrossRef]
83. Delvaux, D.; Sperner, B. New aspects of tectonic stress inversion with reference to the TENSOR program. *Geol. Soc. Lond. Spec. Publ.* **2003**, *212*, 75–100. [CrossRef]
84. Delvaux, D.; Barth, A. African stress pattern from formal inversion of focal mechanism data. *Tectonophys* **2010**, *482*, 105–128. [CrossRef]
85. Delvaux, D. Release of program Win-Tensor 4.0 for tectonic stress inversion: Statistical expression of stress parameters. In Geophysical Research Abstracts, Proceedings of the EGU General Assembly, Vienna, Austria, 22–27 April 2012; EGU: Munich, Germany; Volume 14, p. 5899. Available online: https://www.researchgate.net/publication/258618974 (accessed on 1 January 2022).
86. Carey, E.; Brunier, B. Analyse théorique et numérique d'un modèle méchanic élémentaire appliqué à l'étude d'une popula- tion de failles. *Comptes Rendus Acad. Sci. Paris* **1974**, *279*, 891–894.
87. Angelier, J. Determination of the mean principal directions of stresses for a given fault population. *Tectonophys* **1979**, *56*, T17–T26. [CrossRef]
88. Bott, M.H.P. The mechanics of oblique slip faulting. *Geol. Mag.* **1959**, *96*, 109–117. [CrossRef]
89. Angelier, J. Fault slip analysis and palaeostress reconstruction. In *Continental Deformation*; Hancock, P.L., Ed.; Pergamon Press: Oxford, UK, 1994; pp. 53–100.
90. Lisle, R.J. A critical look at the Wallace-Bott hypothesis in fault-slip analysis. *Bull. Soc. Geol Fr.* **2013**, *184*, 299–306. [CrossRef]
91. Angelier, J. From orientation to magnitudes in paleostress determination using fault slip data. *J. Struct. Geol.* **1989**, *11*, 37–50. [CrossRef]
92. Gephart, J.; Forsyth, D. An improved method for determining the regional stress tensor using earthquake focal mechanism data: Application to the San Fernando earthquake sequence. *J. Geophys. Res.* **1984**, *89*, 9305–9320. [CrossRef]
93. Vandycke, S.; Bergerat, F. Tectonique de failles et paléo-contraintes dans les formations crétacées du Boulonnais (Nord France). *Bull. Soc. Geol. Fr.* **1992**, *163*, 553–560.
94. McFarland, J.M.; Morris, A.P.; Ferrill, D.A. Stress inversion using slip tendency. *Comput. Geosci.* **2012**, *41*, 40–46. [CrossRef]
95. Ouguir, H. Analyse Sédimentologique, Structurale et Lithogéochimique de la Série du Proterozoique Supérieur (PII) de L'environnement de la Mine D'argent D'imiter (Ant-Atlas Oriental, Maroc): Implications Dynamiques. Ph.D. Thesis, Institut National Polytechnique de Lorraine, Nancy, France, 1991. Available online: https://hal.archives-ouvertes.fr/tel-01752165/ (accessed on 1 January 2022).
96. Hejja, Y.; Baidder, L.; Ibouh, H.; Nait Bba, A.; Soulaimani, A.; Gaouzi, A.; Maacha, L. Fractures distribution and basement-cover interaction in a polytectonic domain: A case study from the Saghro Massif (Eastern Anti-Atlas, Morocco). *J. Afr. Earth Sci.* **2020**, *162*, 103694. [CrossRef]
97. Ellero, A.; Malusa, M.G.; Ottria, G.; Ouanaimi, H.; Froitzheim, N. Transpressional structuring of the High Atlas belt, Morocco. *J. Str. Geol.* **2020**, *135*, 104021. [CrossRef]
98. Soulaimani, A. Interactions Socle/Couverture Dans L'Anti-Atlas Occidental (Maroc) : Rifting Fini-Proterozoique et Orogenese Hercynienne. Ph.D. Thesis, Université de Marrakech, Marrakech, Morocco, 1998; p. 214.
99. Soulaimani, A.; Burkhard, M. Late Neoproterozoic carbonate productivity in a rifting context: The Adoudou Formation and its associated bimodal volcanism onlapping the western Saghro inlier, Morocco. *Geol. Soc. Lond. Spec. Publ.* **2008**, *297*, 285–302. [CrossRef]
100. Soulaimani, A.; Michard, A.; Ouanaimi, H. Late Ediacaran-Cambrian structures and their reactivation during the Variscan and Alpine cycles in the Anti-Atlas (Morocco). *J. Afr. Earth Sci.* **2014**, *98*, 94–112. [CrossRef]
101. Mrini, Z. Chronologie (Rb-Sr, U-Pb), Chronologie (Rb-Sr, U-Pb), Traqage Isotopique (Sr-Nd-Pb) des Sources de Roches Magmatiques Kburnkennes, Panafricaines et Hercyniennes du Maroc. Ph.D. Thesis, Université Cadi Ayad, Marrakech, Morocco, 1993; p. 200.
102. Azizi Samir, M.R.; Ferrandini, J.; Tane, J.L. Tectonique et volcanisme tardi-Pan Africains (580-560 M.a.) dans l'Anti-Atlas Central (Maroc): Interprétation géodynamique à l'échelle du NW de l'Afrique. *J. Afr. Earth Sci.* **1990**, *10*, 549–563. [CrossRef]
103. Soulaimani, A.; Essaifi, A.; Youbi, N. Les marqueurs structuraux et magmatiques de l'extension crustale au Protérozoïque terminal—Cambrien basal autour du massif de Kerdous (Anti-Atlas occidental, Maroc). *Comptes Rendus-Geosci.* **2004**, *336*, 1433–1441. [CrossRef]
104. Soulaimani, A.; Bouabdelli, M. L'extension continentale au Néo-Protérozoïque supérieur-Cambrien inférieur dans l'Anti-Atlas (Maroc). *Bull. Soc. Geol Fr.* **2003**, *174*, 83–92. [CrossRef]
105. Benssaou, M.; Hamoumi, N. Le graben de l ' Anti-Atlas occidental (Maroc): Contrôle tectonique de la paléogéographie et des séquences au Cambrien inférieur The Lower-Cambrian western Anti-Atlasic graben: Tectonic control of palaeogeography and sequential organisation. *Comptes Rendus-Geosci.* **2003**, *335*, 297–305. [CrossRef]
106. Lower Palaeozoic of North-Western and West Central Africa. Holland, C.H. (Ed.) John Wiley: New York, NY, USA, 1985; pp. 91–336.
107. Buggisch, W.; Flügel, E. The Precambrian/Cambrian boundary in the Anti Atlas (Morocco). Discussion and new results. *Lect. Notes Earth Sci.* **2006**, *15*, 81–90. [CrossRef]
108. Raddi, Y.; Baidder, L.; Michard, A.; Tahiri, M. Variscan deformation at the northern border of the West African Craton, eastern Anti-Atlas, Morocco: Compression of a mosaic of tilted blocks. *Bull. Soc. Geol Fr.* **2007**, *178*, 343–352. [CrossRef]

109. Soualhine, S.; León, J.T.D.; Hoepffner, C. Les faciès sédimentaires carbonifères de Tisdafine (Anti-Atlas oriental): Remplissage deltaïque d'un bassin en «pull-apart» sur la bordure méridionale de l' Accident sud-atlasique. *Bull. L'institut Sci. Rabat Sect. Sci. Terre* **2003**, *25*, 31–41. Available online: https://www.researchgate.net/publication/238083700 (accessed on 1 January 2022).
110. Houari, M.R.; Hoepffner, C. Late Carboniferous dextral wrench-dominated-transpression along the North African craton margin (eastern High Atlas, Morocco). *J. Afr. Earth Sci.* **2003**, *37*, 11–24. [CrossRef]
111. El Arabi, E.H.; Diez, J.B.; Broutin, J.; Essamoud, R. First palynological characterization of the middle Triassic; implications for the first Tethysian rifting phase in Morocco. *Comptes Rendus-Geosci.* **2006**, *338*, 641–649. [CrossRef]
112. Frizon de Lamotte, D.; Leturmy, P.; Missenard, Y.; Khomsi, S.; Ruiz, G.; Saddiqi, O.; Guillocheau, F.; Michard, A. Mesozoic and Cenozoic vertical movements in the Atlas system (Algeria, Morocco, Tunisia): An overview. *Tectonophysics* **2009**, *475*, 9–28. [CrossRef]
113. Hailwood, E.A.; Mitchell, J. Paleomagnetic and radiometric dating results from Jurassic intrusions in South Morocco. *Geophys. J. R. Astron. Soc.* **1971**, *24*, 351–364. [CrossRef]
114. Sebai, A.; Feraud, G.; Bertrand, H.; Hanes, J. 40Ar/39Ar dating and geochemistry of tholeïtic magmatism related to the early opening of the Central Atlantic rift. *Earth Planet. Sci. Lett.* **1991**, *104*, 455–472. [CrossRef]